Dissolved trace elements dynamics during a rich-CO2-water leakage in a near-surface carbonate freshwater aquifer

Léna Rossi, Corinne Loisy, Adrian Cerepi, Anélia Petit, Olivier Le Roux, Audrey Estublier, Sonia Noirez, Frédéric Martin, Benoit Hautefeuille, Thomas Brichart, et al.

Dissolved Trace Elements dynamics during a rich-CO_2-water leakage in a near-surface carbonate freshwater aquifer

Léna Rossi[1*], Corinne Loisy[1], Adrian Cerepi[1], Anélia Petit[1], Olivier Le Roux[1], Audrey Estublier[2], Sonia Noirez[2], Frédéric Martin[2], Benoit Hautefeuille[3], Thomas Brichart[3], Bruno Garcia[2]

[1] EA 4592 « Géoressource & Environnement », ENSEGID - Bordeaux INP, Avenue des Facultés, CS 60099, 33 400, Talence, France

[2] IFP Energies Nouvelles, 1 & 4 avenue du Bois Preau, 92852, Rueil-Malmaison, France

[3] GLINCS S.A.S-L'Atrium, 43 Boulevard du 11 Novembre 1918, 69100, Villeurbanne, France

Corresponding author: lena.rossi@bordeaux-inp.fr

Abstract:

An experimental leak "simulation" was carried out at the Saint-Emilion experimental site (France). A volume of 200 L of CO_2-rich water was injected into the shallow carbonated aquifer during low water table periods. One injection well and seven monitoring wells were equipped with either CO_2 probes or multi-parameters probes to follow the plume.

After the CO_2-rich water injection, dissolved CO_2 and electrical conductivity increased as the pH values decreased, highlighting the calcite dissolution. The calcite dissolution and desorption of iron oxides led to the migration of trace elements in the aqueous phase. As, V, Mo Cu, Ga, Co, Fe, and Cd showed a rapid increase in their concentrations. Mn, Sr, Li and Se showed the same evolution but with a temporal offset. The concentrations of some of these elements increased a second time several hours after the injection. Ba and Pb showed a major decrease immediately after injection, but Ba showed two peaks several hours after the injection. Zn and Si seemed to not be affected by the CO_2 injection.

Only As, Ba, and Se exceeded WHO/UE drinking water standards for a period of few hours. The global return to initial conditions was fast, showing the great resilience and the high buffering capacity of carbonate aquifers.

Keywords: CO_2 leakage, Shallow carbonate freshwater aquifer, CO_2-rock-water interactions, Field experiment, CO_2 geological storage, Trace Elements

48 # 1 Introduction

49

50 The international community awareness and the scientific data on global warming
51 confirm the urgency of the deployment of technologies to reduce greenhouse gas emissions.
52 At this time, CO_2 capture and storage (CCS) is a major scientific and technical issue and is a
53 well-known and well-studied option for the past few years (IPCC, 2005). This technology
54 involves the capture of the CO_2 from an industrial source and its transport of CO_2 to an
55 injection site to store it for long-term in the deep underground geologic formations such as
56 depleted oil and gas fields or saline aquifers (IPCC, 2005) that meet several criteria of
57 injectability, storage capacity, and integrity (Bachu, 2008). The injected CO_2 is then
58 progressively trapped by physical trapping mechanisms (i.e., when the CO_2 is immobilized as
59 free gas or supercritical fluid) and chemical trapping mechanisms (i.e., when the CO_2
60 dissolves in subsurface fluids or adsorbs onto organic materials contains on coals and shales
61 for example) (Bachu, 2008; Golding et al., 2011; Gunter et al., 2004; Zevenhoven et al.,
62 2006). The main risk associated with geological storage are leakages which may occur during
63 the process of injection (Damen et al., 2006) and/ or after, along with faults and fractures
64 networks (Farret and Thoraval, 2013; Ringrose et al., 2009) or by the alteration induced by
65 CO_2-water-rock interaction.

66 One of the major concerns is the possibility of CO_2 leakage to an underlying shallow
67 freshwater aquifer, causing a change of chemical equilibrium between the gas, the water, and
68 the rock of the aquifer, that could potentially lead to pollution of water resources due to the
69 release of trace elements contained in the rock (Harvey et al., 2012; Jones et al., 2015;
70 Lemieux, 2011; Lions et al., 2014; Qafoku et al., 2017). Over the last decade, many studies
71 have been completed to understand the chemical processes involved in releasing trace
72 elements of CO_2 leaks in groundwater. Different types of approaches covering a wide

spectrum of spatial and temporal scales like laboratory experiments (Cahill et al., 2013; Humez et al., 2013; Lawter et al., 2018; Little and Jackson, 2010; Montes-Hernandez et al., 2013; Wunsch et al., 2014), field tests (Cahill and Jakobsen, 2013; Gal et al., 2013; Gal et al., 2014; Giese et al., 2009; Kharaka et al., 2010; Rillard et al., 2014; Trautz et al., 2013; Yang et al., 2013; Zhu et al., 2015), modeling studies (Apps et al., 2011; Bacci et al., 2011; Bacon et al., 2016; Tambach et al., 2011; Zheng et al., 2016) and natural analogs studies (Do et al., 2020; Keating et al., 2010) are discussed in the literature. Laboratory experiments are the main type of approach to study the gas-water-rock interactions as they permit the reproduction of these interactions under controlled conditions thus simplifying their understanding. Some of these have focused on rocks with varying carbonate contents. For example, Cahill et al., (2013) investigated risks due to water quality changes in shallow drinking aquifers from leakage of geological carbon sequestration in sediments of variable carbonate content *via* batch experiments. Lawter et al., (2018) studied the element mobilization and immobilization from carbonate rocks *via* batch experiment. They focused on the intermediate zone between CO_2 storage reservoirs and the overlying aquifers. Wang et al., (2016) worked on the geochemical impacts of CO_2 leakage to an unconfined oxidizing carbonate aquifer via batch and column experiments. Conversely, Wunsch et al., (2014) performed laboratory batch experiments to analyze the potential for trace element release due to carbonate mineral dissolution in limestone aquifers. However, these experiments have the disadvantage of not reproducing the geological physical (i.e., petrophysical rock properties and hydrodynamics properties of the aquifer) and chemical natural complexity of the aquifer and their heterogeneity.

Among the experiments carried out on a field scale, there are some which focus on CO_2 leak experiments in a shallow aquifer. To date, much of these field experiments have focused on siliciclastic aquifers with little carbonate content. For example, Yang et al., (2013) have

carried out a single-well push-pull test for assessing potential impacts of CO_2 leakage on groundwater quality in a shallow Gulf Coast aquifer in Cranfield (Mississippi). In this study, 3825 L of gasified water was injected into a sand and clay aquifer. Cahill and Jakobsen, (2013) conducted a shallow CO_2 injection experiment in an unconfined, unconsolidated aquifer however, the aquifers were mainly siliciclastic. Rillard et al., (2014) performed a shallow push-pull field experiment to assess the geochemical impact of a CO_2 perturbation but in a fractured sandstone aquifer. To the best of our knowledge, no field experiment assessing the geochemical impact of a CO_2 leak in an exclusively carbonate near-surface freshwater aquifer has been conducted to date.

As trace elements are also present in the crystalline structure of carbonate minerals (Thorstenson and Plummer, 1977; Zachara et al., 1991) they can therefore be released into the aqueous phase during their dissolution and constitute a risk for the quality of drinking water. Moreover, carbonated aquifers are well represented around the world and 20 to 25% of the population uses the carbonate aquifer as a drinking water resource, and may therefore be subject to CO_2 intrusion in the case of a leak (Ford and Williams, 2007). Furthermore, the literature has shown that the effects of CO_2 leakage are site-specific (Zheng et al., 2015). The impact depends on the sedimentary formations, hydrogeology context, and geochemistry of the aqueous phase, implying that the extrapolation of the results for other sites is not possible. Studies are still needed to extend the comprehension of the effects of a CO_2 leak on water quality and finally to increase acceptance of this technology.

This work is part of the *Aquifer-CO_2-Leak Project* and follows the work of Gassara et al., (2021) on the pre-dimensioning of the experiment by numerical modeling of CO_2 leakage and the work of Petit et al., (2021) on the characterization of the physicochemical impact of the injection of CO_2-rich water in the carbonate aquifer of Saint-Emilion (France). The objective of this study is to understand, quantify and evaluate the impact of a CO_2-rich water

123 leak on water quality and more specifically on the dynamics of dissolved trace elements in a
124 shallow freshwater carbonate aquifer with a very high calcite content of 98 ± 2% $CaCO_3$
125 (Loisy et al., 2013). The objective is to acquire in situ data that would serve to identify and
126 quantify trace elements concentrations which in turn could serve to model chemical
127 mechanisms responsible for trace elements mobilization at a small experimental site scale.
128 This paper first presents the geological and hydrogeological context of the study,
129 followed by the results of the rock characterization and the geochemical monitoring of the
130 CO_2-rich water plume over time. Finally, these results are interpreted and discussed.
131

132 ## 2 Materials and methods

133 ### 2.1 Geographical, geological, and hydrological context of the study site

134

135 The experimental site is in an underground limestone quarry at Saint-Emilion, in the
136 New Aquitaine region (France) (**Fig.1a**). The quarry is in a limestone formation dating from
137 the Upper 1b Oligocene (Stampien; 28-30 Ma) and exploited on two levels (to 8 and 16 m
138 deep on average) according to the "rooms and pillars" method (Loisy et al., 2013). The
139 limestone formation of around 25 meter-thick is characterized by carbonate and biodetritic
140 facies. This formation mainly consists of grainstone to wackestone facies (Dunham, 1962)
141 and is associated with high values of porosity (28.5 to 41.5%) and permeability (4.3 and 11.8
142 D) according to a previous study taken place in the quarry (Cohen et al., 2013; Loisy et al.,
143 2013; Rillard et al., 2015). Previous calcimetry measurements revealed a $CaCO_3$ content of
144 the limestone of about 98% ± 2% (Rhino et al., 2016). Previous studies have highlighted that
145 the porosity is only represented by the matrix pore network because all fractures present in the
146 formation are filled by impermeable red clays (Cerepi et al., 1998) and that the heterogeneity

147 of the pore structure and/or the alteration of the rock explained the high range of values
148 (Rillard et al., 2014).

149 In the area of the experimental site, the hydrogeological system is composed of 0.30
150 m of soil (Combisol calcalric type; IUSS Working Group WRB, 2007) and 21 m of Oligocene
151 limestone of which approximately 3 m rests in the saturated zone, depending on the aquifer
152 recharge (**Fig.1a**). The water table is located at the lower part of Oligocene limestones and
153 above levels of impermeable Sannoisian green marls (Vincent and Maton, 1999; Vouvé,
154 1990). Its drainage axis is NW-SE orientation. The range of the hydraulic gradient is between
155 2% at the lowest water table elevation to 5% at the highest water table elevation. At the time
156 of this experiment, the hydraulic gradient was 2% with a water table elevation of 61.35 m
157 NGF (General Levelling of France;) (**Fig.1a**). Groundwater resource is fed directly by
158 meteoric water. The flows are vertical and controlled by gravity and the downward
159 percolation takes place via the pillars of the quarry (Loisy et al., 2013).
160

161 ## 2.2 Experimental methodology

162 ### *2.2.1 Experimental site and injection of the CO_2-rich water*
163

164 The pilot site is located approximately 16 m deep at level 2 of the quarry (**Fig.1a, b).**
165 To carry out the CO_2-rich water injection experiment, eight boreholes of 8 cm in diameter,
166 between 4.8 and 6.0 m deep were drilled along the hydraulic gradient (an injection well-
167 named F1 and seven observation wells named from F2 to F8; **Fig.1b**) on 7.10 m of distance
168 (i.e., between F1-F8). A PVC tube was placed on the upper part of the borehole to reinforce
169 the backfill (**Fig.1c**). The drilling was carried out using a destructive technique using water

from the boreholes to drill and cool the machine to minimize the disturbance to the system. Only one borehole (F2) has been used for taking core samples.

A 200 liters volume of Oligocene aquifer water drawn and stocked in a stainless tank was used for the water gasification and then the injection. A motor, pressure sensors, and an output flow meter were added to the tank to control the gasification and injection processes. The gas bottle of 50 L composed of a mixture of CO_2 (90 %), He (9%), Kr (1%) was bubbled in the tank with fluorescent molecules (fluorescent based Lanthanide, used as an inert tracer) about 24 hours until saturation. The rich-CO_2-water injection started on July 09th, 2019, at 10 a.m in the well F1, and lasted approximately 30 minutes. This corresponds to the time of the experiment which will be taken as a reference to describe the results. During this first step of the leak simulation, the dissolution of the CO_2 did not take place in the aquifer itself but the tank. We have chosen to not inject CO_2 directly into the aquifer to control all the physical and chemical parameters of the input signal. The end of the monitoring of all parameters combined is dated August 01st, 2019. The injection velocity was 2.20 L/min and was chosen as it was close to the speed of the water table. This made it possible to avoid hydraulic overload and a piston effect on water dynamics. The physicochemical parameters of the tank water are presented in **table 1**.

2.2.2 Physicochemical parameters monitoring

Four CO_2 probes of the CO_2-Pro ™ type (Pro Oceanus) (± 2% (Pco_2 10-900 mbar)) and four multi-parameter probes of the Aqua TROLL 600 Multiparameter Probe type were respectively introduced into wells F1, F2, F3 and F6 and F1, F3, F6, and F8 (**Fig.1b**). These probes were immersed continuously in the aquifer and recorded physicochemical parameters every 30 min such as electrical conductivity (± 0.5% of reading plus 1.0 µS/cm), pH (± 0.1

195 pH units), oxidation-reduction potential (ORP, ± 0.5 mV), and temperature (± 0.1 °C). During
196 the experiment, the multi-parameter probe in F1 was moved to well F8 after that the
197 parameters had returned to the baseline in F1. The probes were isolated from the quarry
198 atmosphere by packers (or inflatable stoppers) designed and produced especially for this
199 experiment. They were kept inflated throughout the experiment using a compressor and a gas-
200 tight tubing system hung from the quarry ceiling (**Fig.1b, c**).

201

202 *2.2.3 Sampling strategy*

203

204 All wells were equipped with water sampling tubing at two depths below the level of
205 the water table (about 25 and 70 cm below, respectively 61.10 m NGF, and 60.65 m NGF for
206 the well F1) to check if there were differences in concentrations on this scale. Previously,
207 Petit et al., (2021) concluded that there were no significant differences between these two
208 depths. Therefore, the results will be presented for one depth (25 cm below the level of the
209 water table).

210 The water samples were taken using a type Ismatec® water pump connected to the
211 tubing of each well. According to the pump flow rate and the volume contained in the pipe,
212 one minute was necessary to purge the pipe. The water was collected in a beaker previously
213 rinsed three times with the water withdrawn. Given the increased risk of degassing, pH,
214 conductivity, and temperature were measured immediately after the sampling directly in the
215 beaker using a Consort C561 multiparameter analyzer. A volume of 15 ml of water for the
216 analysis of trace elements was taken from the beaker and filtered using a 0.2 µm nylon filter
217 and placed in a 16 ml borosilicate glass vial previously decontaminated with aqua regia 5%
218 (HNO_3 67-69%, Trace Metal ™ and HCl 37%, Trace Metal Analysis, d = 1.18, Primar Plus

219 ™). Due to poor air renewal in the quarry and for safety reasons, the samples were acidified at
220 the quarry exit (2% - HNO_3 67-69%, Trace Metal ™) approximately one hour after collection.
221 Similarly, two water volumes of 16 ml were taken from borosilicate glass vials for the
222 analysis of cations and anions concentrations and alkalinity analysis. They were directly
223 stored and transported at 4 °C in the dark enclosure to the laboratory until analysis.

224 Samples were taken every 8 hours for the first two weeks, then every 12 hours, and
225 finally every other day at the end of the experiment. Samples were not taken systematically
226 from all wells each time. Sampling was concentrated on the wells according to the plume
227 migration. This sampling strategy was determined following the results of preliminary salt
228 tracing experiments (Petit et al., 2021). Due to the possible degassing, the samples for the
229 cation-anion analysis were filtered with 0.2 µm nylon filters just before their analysis.

230

231 *2.2.4 Rocks samples characterization*

232

233 Six samples of limestone were analyzed to determine their trace elements
234 concentration and their other petrophysical characteristics. Chemical and physical analyses
235 were carried out on grainstone and boundstone facies samples to see their differences. They
236 were sampled from the sediment core collected when drilling in the well F2 at 0.63, 1.15,
237 1.80, 2.22, 3.23, and 4.05 meters from the quarry floor (64.17 m NGF) (**Fig.1a**; **Fig.2a**).
238 Porosity was measured by Hg-injection and permeability was measured by variable head air
239 permeameter methods. The mineralogical composition of the samples was analyzed using the
240 X-ray diffraction (XRD) type D8 Advance (Brucker). X-ray fluorescence (XRF) analyses of
241 the limestone were carried out using a HORIBA XGT 5000. These analyses made it possible

to obtain semi-quantitative concentrations of the elements constituting a circular target zone (diameter of 100 µm).

Total trace element analyses were carried out using the tri-acid digestion method. After having dried, crushed, and homogenized, a representative aliquot of rocks (i.e. 150 mg) were digested in acid-cleaned closed PP tubes (DigiTUBEs) in a Teflon-coated heating block (2 hours at 110 °C) with 1.5 mL HCl (10 M Suprapur), 750 µL HNO_3 (14 M Suprapur) and 2.5 mL HF (29 M Suprapur), as described in previous studies (Schafer et al., 2002; Gil-Díaz et al., 2018). After evaporation to dryness and re-dissolution of the residue with 250 µL HNO_3 (14 M) in the heating block, the samples were brought to 10 mL using Milli-Q® water. Concentrations of particulate Ag, As, Ba, Cd, Co, Cu, Cr, Mo, Ni, Pb, Sb, Sr, V and Zn were quantified using triple quadripole ICP-MS (iCAP-TQ) using an external calibration. To verify precision and accuracy, the analytical method was quality checked with international certified reference materials (NIST8704; SLRS-6). Concentrations of particulate trace elements such as Be, Fe, Ga, In, Li, Mn, Se and Si of the same samples were quantified using an ICP-AES (iCAP 6000 Series) using external calibration with a multi-element standard solution (Multi-element standards solution 5 for ICP, TraceCERT®).

2.2.5 Water samples characterization

Dissolved trace elements were analyzed using an ICP-AES (iCAP 6000 Series) with external calibration. Blank and standards were analyzed at the same time to control the drift of the ICP-AES. The calibration range varies from 10 to 100 µg/L using a multi-element standard solution (Multi-element standards solution 5 for ICP, TraceCERT®). Major ions were analyzed using an HPLC (High-Performance Liquid Chromatography) of the DIONEX

type, equipped with a CS12A analysis column and an IONPAC® CG12A protection column (mg/L, ± 5%). The device is calibrated to be adapted to the sample matrix. The calibration range varies from 5 to 200 mg/L of $Ca^{2+,}$ Mg^{2+}, Na^{+}, NH_4^{+}, K^{+}, F^{-}, Cl^{-}, PO_4^{3-} and SO_4^{2-}. About 5 ml of standards or previously filtered samples were placed in closed vials. Between each series of 10 samples, blanks and standards were placed to check the stability of the analyses and the drift of the device. The alkalinity of each sample was measured in the laboratory directly after sampling using the Inflection Point Titration Method (USGS, 2012) with a pH-meter (Consort, ± 0.2%) and a titration solution of 0.1 M hydrochloric acid.

3 Results

3.1 Physical and chemical characterization of the Saint-Emilion limestones samples

The sediment core collected in well F2 presents three distinct lithologies (**Fig. 2a**) (Petit et al., 2021, modified). The floor of the site was composed of carbonate rock up to about 58.4 m NGF (i.e., General Leveling of France; official levelling network in metropolitan France), of which about 50 cm on the surface corresponds to backfill due to the accumulation of carbonate powders released during the digging of the quarry when it was in operation. It is in this porous zone of 58.4 to 61.4 m NGF that the water table is located. An impermeable clay zone (Sannoisian green marls) begins at plus or minus 58.4 m NGF.

The macroscopic study of the sediment core revealed grainstone, boundstone, mudstone, wackestone, and packstone facies, which follow one another or alternate them according to the depth. Several sedimentary structures were observed such as the straight structure, the oblique structure, and the cross-bedded structure.

Microscopic analysis of the six samples made it possible to visualize the differences in geometry, size, and distribution in the porosity between two facies (**Fig.2b**). These samples

290 are mainly composed of remains of *foraminifers*, *bioclasts, Lamellibranchia*, *Oncoides*,
291 *Rhodolithes*, *Bryozoans,* and debris of *Echinoderms*. Rare quartz crystals (< 1 %) were
292 observed in all the thin sections whatever the facies. Iron oxides were also observed in lesser
293 quantities (< 0.5%) in the micritic matrix in a diffuse manner, in certain figured elements, or
294 at the edge of pores. The grainstones show sparitic to microsparitic edge cement and the
295 boundstone have sparitic cements partially filling the pores (**Fig.2b**). No internal sediment
296 was observed plating on the edge of the porosities according to the microscopic analysis.
297 The samples show high variability of porosity from 20 to 43% and permeability from 1
298 to 26 D (**Fig.2a)** The results are consistent with other analyses completed on the Saint-
299 Emilion limestone in the past experiments (porosity values between 28.5% and 41.5%, and
300 permeability values between 4.3 and 11.8 D) by Rhino et al., (2016).
301 According to the X-ray diffraction (XRD) analysis, the mineralogical composition of
302 the samples is almost exclusively calcite ($CaCO_3$) with low traces of quartz (SiO_2). The
303 calcite is shown by the presence of the peak located at 29.5° (main calcite peak) and several
304 other peaks. For the quartz, the peak located at 26.8° is also clearly detectable. No peak
305 corresponding to oxides or clays was found. The spectra of the XRD analysis of three powder
306 samples can be shown in the **supplementary materials.1.** These results are consistent with
307 other analyses on the Saint-Emilion limestone for past experiments. Rhino et al., (2016)
308 presented results of calcimetry technics which revealed a $CaCO_3$ content of 98% ± 2%.
309 Auffray et al., (2016) done XRD investigation and showed that the two main phases were
310 $CaCO_3$ and SiO_2. Furthermore, Rock-Eval 6 analysis confirmed that no organic carbon (i.e.,
311 organic matter) was present in their samples and that mineral carbon was only contained by
312 $CaCO_3$. The authors confirmed their results by SEM-EDXS analysis. To conclude, according
313 to the analysis of the limestone of Saint-Emilion, $CaCO_3$ is the main mineralogical phase and

314 SiO_2, as well as the iron oxides observed with the microscope, are less abundant
315 mineralogical phases present in very weak proportions.

316 Analyses (semi-quantitative) of the samples with X-ray fluorescence (XRF) show that
317 Ca, Si, Fe, Mn, K and Al are the major elements while Cu, Ba, Sr, Zn, S, V, Ti and Pt appear
318 to be minor components (**Tab.2**). The results show great variability within the same facies.
319 For example, silica varies between 3.14 and 25.09% in grainstone samples. This variability is
320 also true for the samples of the boundstone and those for all the elements identified by the
321 XRF. Likewise, each element identified varies greatly along the sedimentary column. Thus,
322 there seems to be a spatial geochemical heterogeneity that seems independent of the
323 sedimentary facies.

324 Subsequently, analyses completed using the tri-acid digestion method were carried out
325 to obtain quantitative results. The elements observed (Al, Ti and Pt) during the XRF analyses
326 could not be analyzed using the ICP for lack of standards or methodological concerns. The
327 details of the total trace elements concentrations of the six samples can be found in
328 **supplementary material.2** and the means ± standard deviations for all the samples and for
329 each facies (boundstone and grainstone) are presented in the **Table 3**.

330 The variation in concentrations (i.e., the standard deviation in percent) around the mean
331 for each facies (three samples each) and the two facies together (six samples) was calculated
332 to better compare the differences between the facies and between the elements (**Fig.3**). When
333 we look at the degree of variation around the mean for all together facies, we notice that the
334 elements Ba, Li, Mn, Pb, Sr and Zn vary between 0 and 25%. These results, therefore, show
335 relatively similar concentrations along the sediment column. The degree of variation of the
336 elements Ag, As, Cd, Co, Cr, Fe, Ga, Mo, Ni, Sb, Se, Si and V vary between 25 and 50%
337 around their averages. The concentrations of these elements, therefore, seem to vary over a
338 broad spectrum along the sedimentary column (**Fig. 3**). The degrees of variation around the

mean of the Cu and In concentrations are very strong. The distribution of these elements, therefore, seems to be very uneven in the sedimentary column. When looking at the degree of variation around the mean for the grainstone and boundstone, it varies between 0 and 25% for elements such as Co, Sr and Zn and their respective means are between each facies are similar. Thus, the distribution of these elements is not specific to particular facies. The degree of variation of the elements such as Ag, Ba, Cd, Cr, Cu, Mn, Sb, Si, Ga and V between the grainstone and boundstone are very different. This indicates that these elements are homogeneous in one facies but not in the other. For example, Ag, Cd, Cr, Cu, Mn and Si have a low degree of variation in the grainstone and high in the boundstone. While Ba, Sb and Ga have a greater degree of variation in the grainstone than in the boundstone. Then there are the elements such as Zn, Se, In, Sr and Li, Mo and Pb which have a degree of variation around their similar means, and their respective mean concentrations for each facies are also similar. , In consequence, these elements do not make it possible to geochemically differentiate the boundstone and the grainstone.

3.2 Evolution of the physicochemical parameters in carbonate freshwater aquifer during the experiment

The evolution of the physicochemical parameters of the CO_2-rich water plume over time is presented for the wells F1, F2, F3, F6, and F8 in **Fig. 4**. Baseline measurements of physicochemical parameters recorded up to 25 hours before the injection showed little variation. The physicochemical parameters showed a small heterogeneity according to the baseline values recorded 25 hours before the injection. The pH varied in the range between 7.02 et 7.15 for the wells F1 and F3, the conductivity varied between 632 µS/cm and 738 µS/cm for the wells F3 and F1, the dissolved CO_2 varied in the range between 1.84% and

2.46% for the wells F2 and F1 and the ORP values varied between 233 mV and 376 mV. Finally, the temperature of the water table varied from 13.03 °C for the well F6 to 13.12 °C for the well F1. This baseline recording time was sufficient to avoid confusing the variations induced by the injection of CO_2-rich water with those resulting from the natural annual hydrogeological variability of the water table.

The injection of CO_2-rich water induced a rapid change of the physicochemical parameters of the water table over the first 120 hours as shown in **Fig. 4.** The variations were greater in the injection well F1 than in the others. The injection immediately produced a sharp drop in pH of 1.4 units (from 7.02 to 5.63 post-injection). It returned to its initial value after 40 hours. The other wells showed a lower pH drop, a wider peak, and a more time interval according to their distance with F1. The pH drop in F3 is 0.20 units (from 7.15 to 6.97 post-injection), was 0.07 units (from 7.03 to 6.96 post-injection) in F6, and 0.03 units (from 7.10 to 7.07 post-injection) in the well F8. The minimum pH values were recorded simultaneously with the maximum conductivity values. Conductivity rose from 679 to 1551 µS/cm in the well F1, which records the strongest rise 7 hours after the injection. The increase in conductivity was smaller in the other wells, with a rise from 617 to 729 µS/cm in the well F3, from 665 to 716 µS/cm in the well F6, and from 714 to 777 µS/cm in the well F8.

A rapid rise in dissolved CO_2 from 2.5 to 19.7% was noticeable immediately after the injection in the well F1 with a return to an initial value from 40 hours. The curve of dissolved CO_2 in well F1 showed a plateau due to the saturation of the probe which the range was limited to 20%. The dissolved CO_2 from well F1 was recalculated under PhreeqC software by inverse modeling from the analysis of cations and anions to obtain the maximum values of 30% (Petit et al., 2021). Wells F2 and F3 farther from the injection well showed a lower rise with a wider peak. Dissolved CO_2 increases to 3.54% between 20 and 60 hours in well F2. It rises to 3.67% between 40 and 120 hours in the well F3. The CO_2 probe initially installed in

well F1 was moved to well F8 from 145 hours after the plume of CO_2 had dissipated in F1. Therefore, there are no data for the F8 well before 145 hours. The sudden decrease occurring at this time corresponds to the withdrawal and re-filling of the probe. The arrival of CO_2 occurred between 320 and 340 hours after the start of the injection.

The ORP recording showed minimal values in the F1 injection well while the other wells did not show significant variations after the injection. A temperature rise was only noticeable in the well F1 (14.60 °C after the injection.) Alkalinity (as HCO_3^-) showed the same trend as other parameters with a peak of 832.70 mg/L in F1 with lower peaks in other wells.

From a general point of view, the pH, alkalinity, conductivity, and dissolved CO_2 showed similar temporal offset between each well but there were slight shifts. The highest values for pH, ORP, and temperature were recorded less than 1 hour after injection in well F1 while the conductivity and alkalinity peaks were recorded after 7 hours and dissolved CO_2 between 1 hour and 40 min and 13 hours after injection. The dissolved CO_2 registers a peak 35 hours after injection in well F2. Then the plume moves to F3 and reaches the first peak at 68h after injection, followed by a second weaker peak between 120 and 140 hours after injection. Based on conductivity, the arrival of the plume in well F6 took place 138 hours after injection and 328 hours after injection into well F8.

For more details of the physicochemical parameters evolutions following the injection, see Petit et al., (2021).

3.3 Evolution of the trace elements concentrations variation during the experiment

The evolution of the concentrations of the trace elements over time for the wells F1 to F8 is shown in **Fig.5** and **Fig.6.** The black dashed axis at t_0 indicates the moment of the

414 injection. The grey hatched area of some graphs represents the detection limit of the analytical
415 device. Water samples were taken at two depths (i.e., 25 and 70 cm below the water table,
416 respectively 61.10 m NGF, and 60.65 m NGF for the well F1). Petit et al., (2021) showed that
417 there were no concentrations differences between these two depths for the major elements.
418 The same has been concluded for the trace element concentrations. Results for the depth E2
419 are shown in the **supplementary material.3 and .4**. Furthermore, results for Ag, Sb, In, Ni,
420 and Cr were below or very closer to the detection limits in the majority of the wells and will
421 not be treated in the rest of this study.

422 When looking at the natural pre-injection concentrations for each of the trace
423 elements, these are more or less variable between wells, showing some small-scale
424 geochemical heterogeneity. The results showed that Se, Mn, Mo, Co and Cd concentrations
425 were not detectable with our analysis method in the dissolved phase before the injection of the
426 CO_2-rich water in all the wells. The concentrations of the other elements varied to a greater or
427 lesser extent depending on the well and the element. For example,

428 As varied between 1.60 µg/L (well F4) and 3.37 µg/L (well F5)

429 Ba varied between 9.70 µg/L (well F2) and 1105.45 µg/L (well F7),

430 V varied between 0.89 µg/L (well F5) and 2.11 µg/L (well F8),

431 Sr varied between 118.20 µg/L (well F2) and 182.16 µg/L (well F8),

432 Ga were below the detection limit in the well F4 and F8 and showed a maximum of
433 7.17 µg/L in the well F6,

434 Fe was below the detection limit in the well F1, F2, F4, and F6 and showed a
435 maximum of 129.47 µg/L in the well F8,

436 Pb varied from 2.27 µg/L (well F8) to 7.60 µg/L (well F1),

437 Si varied from 1397.00 µg/L (well F4) and 2233.00 µg/L (well F8),

438 Zn varied between 11.60 (well F2) and 365.30 (well F4), finally,

Li varied between 1.40 (well F2) and 2.07 µg/L (well F8).

After the injection of the CO_2-rich water, the injection well F1 showed higher concentrations. They were close to or under the detection limit in the other wells. In the well F1, Ga, Cu, Fe, Co, and Cd concentrations increased immediately after injection. Ga and Cu had a higher dissolved concentration with a rise respectively to 116.04 µg/L and 22.18 µg/L. Before the beginning of the injection Fe, Co and Cd were not detected. They reached a concentration peak respectively of 57.88 µg/L, 4.65 µg/L and 0.35 µg/L during the injection. After reaching a peak, their concentrations decreased.

The concentrations of As, V and Mo increased immediately after injection in the injection well. They reached a concentration peak respectively of 17.08 µg/L, 11.92 µg/L and 5.01 µg/L. Then, their concentrations decreased but reached a second lower peak a few hours later in the same well. They reached a second peak respectively of 3.11 µg/L after 56 hours, 2.42 µg/L after 48 hours, and 1.51 µg/L after 56 hours after the injection.

The concentrations of Sr, Li, Se, and Mn increased 8 hours after the injection and reached a second peak a few hours later in the injection well. The concentration of Sr increased to 224.26 µg/L and reached the second peak of 129.57 µg/L 48 hours after the injection. The concentration of Li reached the first peak of 2.12 µg/L and the second peak of 1.53 µg/L 48 hours after the injection. Se concentration reached the first peak of 7.70 µg/L and a second of 15.96 µg/L after 56 hours. Then the concentration of Mn increased to 23.46 µg/L and decreased more slowly than the others.

On the overhand, Ba showed two peaks in the well F1 of 1305.50 µg/L after 40 hours and a second of 574.72 µg/L after 128 hours. Also, Ba was detected with high concentrations before injection.

462 Significant concentrations were measured for Pb in the injection well, and a major
463 decrease was recorded immediately after injection. It was detected before the injection but not
464 in all wells and decreased under the detection limit with the injection start.

465 Lastly, Zn and Si concentrations do not appear to be altered after injection in each
466 well. They vary respectively between <0.00 µg/L (all wells) and 1582.90 µg/L (well F6) and
467 723.10 µg/L (well F1) and 3254.10 µg/L (well F4), and. After the injection in the well F1 the
468 concentrations return to concentrations like those of the baseline or concentrations below
469 these except for V, Ga, and Li where their concentrations rise after several days.

470 # 4 Discussion

471 ## 4.1 General changes in groundwater chemistry due to the CO_2 leak in a shallow
472 carbonated system

473

474 The injection of the CO_2-rich water caused a pH immediate decrease simultaneously
475 with the $CO_{2\,(aq)}$ increase in the injection well F1. The dissolved CO_2 caused an increase in the
476 concentration of carbonic acid (H_2CO_3), followed by deprotonation of thereof and further
477 lowering the pH values of the solution, following the simplified equations (Appelo and
478 Postma, 2005):

479 $CO_{2\,(g)} + H_2O_{\,(l)} \rightarrow H_2CO_3^-{}_{(aq)}$

480 $H_2CO_3^-{}_{(aq)} + H_2O_{\,(l)} \rightarrow HCO_3^-{}_{(aq)} + H_3O^+{}_{(aq)}$

481 $HCO_3^-{}_{(aq)} + H_2O_{\,(l)} \rightarrow CO_3^-{}_{(aq)} + H_3O^+{}_{(aq)}$

482 Secondly, the released protons reacted with carbonates and are consumed during their
483 dissolution (Lions et al., 2014; Smith and Mead, 1962). The attenuation of the pH is
484 particularly marked in aquifers rich in carbonates because, in the presence of protons, the
485 dissolution of carbonate minerals is more important. Indeed, the dissolution of carbonate

minerals led to an increase in alkalinity, due to the increase in the concentrations of carbonate and bicarbonate ions, allowing the increase of the buffering capacity of the solution (Lions et al., 2014). Eventually, a physicochemical equilibrium between the CO_2, the rock and the water occurs:

$$CaCO_{3\,(s)} + CO_{2\,(g)} + H_2O_{\,(l)} \leftrightarrow 2\ HCO_3^{-}{}_{(aq)} + Ca^{2+}{}_{(aq)}$$

Thus, the dissolution of calcite was the first phenomenon playing a buffer role on the pH in this aquifer (Qafoku et al., 2017). This effect was also reflected by the increase in pH values and the decrease in dissolved CO_2, alkalinity, and conductivity in well F1 once the peaks passed (**Fig.4**). It should also be remembered that the speed of the water table (0.8 m/day) also played a role in buffering the pH (**Tab. 1**). Our experiment took place in a carbonated aquifer with high values of $CaCO_3$ (98 ± 2%) with a low part of silica and explains the very fast buffering capacity of the aquifer.

Calcite dissolution can also lead to a release of major ions (Petit et al., 2021) and trace elements in the aqueous phase, which can be illustrated by the following relationship (Comans and Middelburg, 1987; Zheng et al., 2016):

$$MCO_{3\,(s)} + H^{+}{}_{(aq)} \rightarrow HCO_3^{-}{}_{(aq)} + M^{2+}{}_{(aq)}$$

The water-rock interface is the site of numerous reactions (e.g. sorption reactions, dissolution and precipitation reactions, ion exchange reactions) (Qafoku et al., 2017). These reactions are in turn influenced by physicochemical parameters (e.g. pH, temperature, redox potential) which will impact the mobility of traces elements (Tanji and Valoppi, 1989). When CO_2-rich water was added to the carbonated system, the physicochemical parameters of the environment changed and led to exchanges between the solid and liquid phases of the aquifer (Harvey et al., 2012). (**Fig.5; Fig.6**). Consequently, the increase of ions in the aqueous phase induced an increase in conductivity in the injection well F1 (**Fig.4**). The changes in oxidation-reduction potential (E_h) are explained by the rich dissolved CO_2 water intrusion (Harvey et al.,

511 2012). The aquifer will be more anaerobic (low E_h) with the entrance of CO_2 and will induce
512 a redistribution of oxidized and reduced species for those which are redox-sensitive in the
513 aqueous phase (Marshall and Fairbridge, 1999). CO_2 intrusion can also induce changes in
514 biological activity (Harvey et al., 2012), but this aspect is not treated in this article.

515 The rise of the temperature only observed in the well F1 is explained by the
516 temperature difference between the water in the aquifer and the CO_2-rich water injected which
517 is in equilibrium with the temperature of the underground quarry. The decrease is explained
518 by the replacement of water coming upstream of the injection point.

519 The heterogeneous nature of the carbonate system was highlighted by the recording of
520 two distinct increases of the conductivity, the pH, and the dissolved CO_2 in well F3. The
521 assumption is that the water upstream arrived via two preferential paths (Petit et al., 2021) due
522 to the heterogeneity of the porosity (also highlighted by Rhino et al., (2016) distinguished two
523 types of porosity for the Saint-Emilion limestone) and permeability of the carbonated system
524 at a small scale.

525

526 **4.2 Trace elements release in the aqueous phase due to the CO_2 leak in a shallow**
527 **carbonated system**

528

529 When looking at the evolution of the trace elements concentrations along the
530 longitudinal axis (F1-F2-F3-F6-F7-F8) and the perpendicular axis (F4-F3-F5) relative to
531 hydraulic gradient, the increase in concentrations occurred significantly only in the injection
532 well F1 (**Fig.4; Fig.5**). Only the concentrations of Se or Sr for example showed a slight
533 increase in the wells F2 and F3. As dissolution only takes place in well F1, advection and
534 dilution dominate the profile of the released elements and diffusion of the plume is not
535 observed in the transverse axis. The low transverse dispersivity is controlled by the

536 petrophysical characteristics and aquifer hydraulic gradient (Gassara et al., 2021). In addition,
537 the high buffering capacity of the limestone in comparison to the small amount of CO_2-rich
538 water injected during this experiment minimizes the dispersion of the plume. This is
539 consistent with the study of the saturation indices by Petit et al., (2021) which showed that the
540 calcite dissolution caused by the CO_2-$CaCO_3$-H_2O reaction only took place in the well F1 and
541 that the variations of the other physicochemical parameters as well as the concentrations in
542 major ions in the other wells were only due to the transport of $CO_{2\ (aq)}$ by advection and
543 diffusion through groundwater flow. However, the behavior of the major ions did not show
544 several peaks or temporal offset as for trace elements, suggesting a more complex chemistry.
545 The lack of concentration differences between the two sampling depths is due to the
546 relative homogeneity of the physical (i.e. hydrodynamic variations) and chemical (i.e.
547 petrography and lithology of the limestone) environment at this scale. However, this is not
548 true on a larger scale as shown by Cahill et al., (2013). Homogenization of the volume of
549 water contained in the well (i.e., 15 L) during injection may also be the cause. Nevertheless,
550 there is some spatial heterogeneity in the chemical composition of the groundwater given the
551 differences in concentrations observed between the wells for the same elements, according to
552 the concentrations before the injection.
553

554 *4.2.1 Origins of the trace elements of the Saint-Emilion limestone*
555

556 According to the analysis of the limestone of Saint-Emilion, $CaCO_3$ is the main
557 mineralogical phase. SiO_2, as well as the iron oxides observed with the microscope, are
558 secondary mineralogical phases present in very weak proportions. The presence of iron oxides
559 in amorphous form would explain that they were not detected with the XRD method and
560 would also explain the number of trace elements detect using the XRF method.

561 Trace elements would be localized in the crystalline structure of carbonate minerals
562 (Thorstenson and Plummer, 1977; Zachara et al., 1991). For example, many trace elements
563 like Ba, Sr (Pingitore and Eastman, 1986), Co, Mn, Zn, and Cd (Comans and Middelburg,
564 1987), Pb (Rouff et al., 2004), Se (Aurelio et al., 2010; Reeder et al., 1994) and or As
565 (Alexandratos et al., 2007; Bardelli et al., 2011) could been incorporated into the cristal lattice
566 during the carbonate sedimentation. Then, the Oligocene limestone, emerged since 32 Ma, has
567 undergone significant meteoric diagenesis and other elements may have been trapped in the
568 cement during this period. Trace elements would be also adsorbed on the iron oxides (Ni et
569 al., 2009; and references therein). During the CO_2-rich water injection experiment, the
570 dissolution processes of carbonates as well as desorption of iron oxides will lead to the release
571 of these trace elements into the aqueous phase.
572

573 *4.2.2 Evolution of the trace element concentrations in the injection well*
574

575 The dissolved trace elements of injection well F1 could be classified into six different
576 groups according to their behavior after injection (**Fig.7**). Furthermore, the relationships
577 between the alkalinity expressed as the HCO_3^- ion, considered as a marker for the dissolution
578 of carbonates, and the different ions analyzed are shown in **Fig.8** to allow hypotheses to be
579 made as to the mechanism of metal release which would be directly linking to the chemical
580 reactions of calcocarbonic system. According to the evolution of the concentrations of the
581 major ions, showed in Petit et al., (2021) and their correlations coefficients with the alkalinity
582 showed in **Fig.8**, most of the changes of the water chemistry are the result of the dissolution
583 of calcite caused by carbonic acid. Therefore the major constituent elements of the carbonate
584 minerals and their potential cationic and anionic substitutions (Alexandratos et al., 2007;

585 Thorstenson and Plummer, 1977; Zachara et al., 1991) will initially be found in the aqueous
586 phase.

587 First, the group of type 1 is composed of Ga, Cu, Fe, Co, and Cd. Their concentrations
588 increased immediately following the CO_2-rich water injection and decreased in the same
589 manner, implying that the mobilization mechanisms of these elements could be similar. Their
590 relationship with the alkalinity is strong. The correlation coefficient (R^2) with the alkalinity is
591 0.92 for Ga, 0.95 for Cu and 0.88 for Co. This suggests that the release of these elements is
592 directly related to the dissolution of calcite. The correlation coefficients for Fe and Cd could
593 not be calculated due to a large number of data below the detection limits. Wunsch et al.,
594 (2014) also showed that Co was released into the solution through calcite dissolution. The
595 Saint-Emilion limestone also contains SiO_2 and iron oxides which were observed in lesser
596 quantities (< 0.5 %) in the micritic matrix in a diffuse manner, in certain figured elements, or
597 at the edge of pores. The release of these elements may be due to a desorption reaction
598 occurring at the same time as the dissolution of carbonates. This was also shown by Cahill et
599 al., (2013) in batch experiments conducted on samples with variable content of $CaCO_3$. Iron
600 concentrations were associated with the presence of ferrihydrite and gibbsite in the sediments.
601 The authors concluded that the weak increase of the aqueous Fe concentration was due to the
602 high buffering capacity of calcite and the pH-dependence of these minerals. This could
603 explain the low concentration of iron in solution compared to its proportion in the Saint-
604 Emilion limestone. Furthermore, the lower pH (e.g pH 5.45) of the injected solution may have
605 also led to the initial dissolution of the iron oxides and explained the initial increase in Fe in
606 the injection well F1.

607 Type 2 is composed of As, V, and Mo. Their concentrations increased directly after
608 the injection as type 1. The correlation coefficient of As with the alkalinity is 0.98 and
609 suggests a mechanism of release similar to type 1. However, Wunsch et al., (2014) also

showed that As had the same tendency as calcium, markers of calcite dissolution, but they finally concluded that the aqueous As concentration was due to desorption mechanisms of arsenate and arsenite, known to can be also incorporated in calcite (Alexandratos et al., 2007; Bardelli et al., 2011). The correlation coefficient with the alkalinity of V and Mo are 0.23 and 0.76, suggesting that the calcite dissolution do not control these elements into solution.

Type 3 is composed of Sr, Li, Mn, and Se. The maximum concentration of these elements was not recorded directly after the injection as for types 1 and 2 but after a temporal offset of 8 hours. Li, Mn and Se showed a weak correlation coefficient with the alkalinity which are 0.44 for Li, 0.50 for Mn, and 0.44 for Se, suggesting that the calcite dissolution was not at the origin of this elements into the aqueous phase. Only Sr has a strong correlation coefficient of 0.96 with the alkalinity (**Fig.8**). An example of carbonate dissolution modeling including only Sr as $SrCO_3$ is shown in **Fig. 9**. The concentrations of Ca^{2+}, HCO_3^- and Sr obtained by modeling are consistent with the experimental results. These results and the strong correlation with the alkalinity suggest that Sr is controlled by carbonate dissolution and precipitation. This modelling work will further explore precipitation and sorption reactions in the future by including all trace elements. These results are also consistent with other studies (Cahill et al., 2013; Wunsch et al., 2014) where aqueous Sr concentrations increased directly with CO_2 exposure. The authors also concluded that the release of Sr was due to calcite dissolution.

Trace elements of types 2 and 3 showed a second peak between 48 and 56 hours after the injection. Limestones present a certain physical heterogeneity due to the double matrix porosity coupled with the creation of preferential paths due to the meteoric diagenesis of dissolution. This physical heterogeneity can have consequences on the dynamics of transport. However, this behavior is not observed in major ions (Petit et al., 2021).

634 The decrease in concentrations suggests the trapping of trace elements by reverse
635 reactions like precipitation or adsorption as carbonate minerals, hydroxides or through
636 sorption. It is also possible that the hydraulic gradient of the aquifer was at the origin of the
637 water renewal in the well F1 and therefore of the dilution of the concentration.

638 The group of type 4 is composed of Pb which showed a major decrease in their
639 concentration immediately after injection. The fact that they were detected before the
640 injection suggests that these elements are scavenged immediately after their migrating onto
641 the aqueous phase. For example, Gheno et al., (2012) have shown that Pb was potentially
642 directly trapped by adsorption reactions with Fe and Mn oxyhydroxides released in the
643 aqueous phase. This could explain the abrupt decrease of Pb at the time of injection until its
644 depletion.

645 Type 5 is only composed of Ba. It can initially be considered as being of type 4
646 because it decreases directly after the injection of CO_2 as Pb but the concentration in the
647 aqueous phase increased after several hours (**Fig.6; Fig.7**). Also, the relationship between
648 alkalinity and Ba concentrations does not show a high correlation ($R^2 = 0.01$) (**Fig.8**) which
649 means that calcite do not control the Ba concentration in the aqueous phase, although it is
650 known that Ba is often present in the crystalline structure of carbonates (Dickens and Bowen,
651 1971; Saito et al., 2020). Some studies have shown that dissolved Ba concentrations increased
652 with the intrusion of the CO_2-rich water plume (Cahill et al., 2013; Trautz et al., 2013;
653 Wunsch et al., 2014), but this is not happening in our case. This suggests that Ba is trapped
654 directly after the limestone dissolves by associating with other elements before being released.

655 Lastly, Zn and Si concentrations do not seem to be affected by the rich-CO_2 water
656 injection and constitute type 6 behavior. These two ions did not seem to show peaks but show
657 great variability in their concentration, which was completely anarchic over time. Either these
658 two elements have their behaviors naturally and the injection does not play any role in the

variations in their concentration, or the mechanisms are very complex, and we have sporadic release elements. Shao et al., (2020) showed in their experiment the same behavior for Zn while Wilkinson et al., (2020) show that Zn is strongly correlated with Ca and has the same behavior as type group 1. This highlights the difficulties to compare studies with each other's as the amount of trace elements released in the aqueous phase will depend essentially on the initial amount of trace elements present in the rock in the solid-state and the hydrogeological context of the site. Therefore, it is important to carry out investigations before setting up CO_2 storage systems.

4.3 Water quality impact

4.3.1 Comparison of total content to the maximum released elements

It is possible to look at which elements are present and which are more easily mobilized by the CO_2 exposure conditions by comparing the maximum concentration observed in the aqueous phase to the total concentration present in the sediment. **Table 3** shows a mean of total trace elements concentrations present in the six limestone samples and the maximums trace elements dissolved concentrations observed for the F1 injection well during the experiment. Results from Baptiste Auffray, (2014) thesis work on limestone come from Saint-Emilion quarry and Lavoux carbonate samples are also included to compare.

The elements that migrate the most in the aqueous phase are not those present in greater quantities in the rock. For example, the samples contain an average of 158.22 mg/kg of Si and only 1.52% has migrated into the aqueous phase while they contain on average 5.64 mg/kg of Ba and 23.15% has passed into the aqueous phase. This shows that the amount of trace elements does not control the water chemistry, which is mainly controlled by the

683 reactivity of the minerals in the rock and the speciation of the elements in the aqueous phase
684 after injection of CO_2-rich water. This also explains the fact that some species in large
685 quantities in the rock are not released in large quantities in the aqueous phase, like Fe.
686 Furthermore, the high buffer capacity of the carbonate aquifer could also limit the carbonate
687 dissolution and the released of trace elements into the aqueous phase.
688

689 *4.3.2 Comparison of the total content of trace elements in the Saint Emilion limestones*
690

691 Total trace elements concentrations in the six limestone samples are in adequacy with
692 the scientific literature of Graf (1962) and Thompson et al., (1970) which synthesize the
693 chemical composition of several carbonate rocks of different ages, facies, and origins. Only
694 Ba, Fe, Mn Si, and Sr total concentrations appear to be a little low than the majority of
695 limestone samples studied (Thompson et al., 1970). In our study, analyzes carried out on the
696 rock samples showed that certain elements distribution was heterogeneous over the entire
697 sedimentary column. The difference in the homogeneity along with the sediment core
698 between elements such as Ba, Li, Mn, Pb, Sr and Zn, more homogeneous and Ag, As, Cd, Co,
699 Cr, Fe, Ga, Mo, Ni, Sb, Se, Si and V, less homogeneous can be explained by returning to the
700 formation of the rock during the Upper 1b Oligocene. The former such as Sr and Ba are
701 markers of marine sedimentation while the others are markers of erosion. However, it is
702 important to remember that only six samples from a core over 4 m long were taken and
703 analyzed. In the end, visibility is low when it comes to the variation in concentrations along
704 the sedimentary column. Likewise, each facies is only represented by three samples. The
705 hypotheses of variations in concentrations within the same facies, suggesting that this makes
706 it possible to discriminate by their geochemical composition, nevertheless remain open to

criticism. It would therefore be interesting in future work to perform additional analyzes on other samples from the same core to complete these results.

However, it is not possible to advance these conclusions for the entire carbonate system of Saint-Emilion. Auffray, (2014) (**Tab.3**) showed results that highlight higher concentrations in general. Except for the elements Sb, Cu, Co, Cd, As and Ag which seem to be in relatively similar orders of magnitude. This comparison between F2 samples and Auffray's samples is possible as the samples come from the same quarry and analysis methods were similar (Auffray, 2014). Thus, the highest concentrations observed for the rest of the elements highlight the heterogeneity contained within the same carbonate system. This can be explained during the formation of these carbonates. The results obtained on the F2 sediment core are therefore not representative of the entire Saint-Emilion carbonate system. This highlights the advantage of carrying out wider studies as the impact on water quality would not have been the same, even under these injection conditions, if the experiment had been conducted elsewhere. Conducting a large sampling and analysis campaign on the solid phase to be able to circumscribe the heterogeneity of the trace elements content of the rock seems essential. This is all truer when we look at the trace elements concentrations in Lavoux's samples (**Tab.4)** (Auffray, 2014). On another scale, a comparison of the mean total trace elements in the limestone samples from the wells F2 between the boundstone and the grainstone does not show a significant difference: facies do not seem a discriminant factor in the trace element concentrations in this study.

4.3.3 Comparison of the maximum dissolved concentration and the maximum concentrations limits

731 One of the consequences of CO_2 exposure from groundwater is exceeding the
732 environmental quality standards imposed. **Table 4** compares the maximum dissolved
733 concentrations of traces elements obtained in well F1 with environmental quality standards
734 for drinking water destinations according to (1) annex I of the decree of January 11th, 2007,
735 relating to the limits and quality references of raw water and water intended for human
736 consumption modified by the decree of August 4, 2017, and (2) the decree of December 9th,
737 2015 (INERIS, 2018) and guide values assigned to natural chemicals whose presence in
738 drinking water is important from a health point of view (WHO, 2017) and quality references
739 for irrigation waters (Ayers and Westcot, 1976). Results showed (at the well F1 scale) that As,
740 Ba, and Se exceeds UE standards, but they return to background concentrations in
741 approximately 20 hours. The return to normal conditions was fast. The carbonated system has
742 great resilience. The small quantity of carbonated water injected combined with the strong
743 buffering capacity of the carbonate system has made it possible to limit the risk of exceeding
744 environmental quality standards and to make the limits short-lived. No concentrations
745 exceeded irrigation water quality standards. Despite these results, it is important to emphasize
746 that the impact would not have been the same under other conditions. However, other studies
747 like Kharaka et al., (2010) have shown that the rise of major ions like Ca, Mg, K, and Na and
748 metal elements like Ba in the aqueous phase, even if they do not exceed the limits standards
749 can also compromise the potable water quality due to their contributions to total dissolved
750 solids (Kharaka et al., 2010). Admittedly, the impact on the quality of the water of our
751 experiment is weak but it is about condition near the surface with a relatively low volume of
752 carbonated water. We must put ourselves back in the context of storage of millions of tonnes
753 of CO_2 and a leak that can last over time. Furthermore, the limits and quality reference are for
754 a large-scale aquifer and here we just discuss it at a very local scale (i.e., a few meters around

755 the injection well). Therefore, modeling from field data could be an interesting tool to provide
756 an overview of the modifications at a more important scale and under more drastic conditions.

757 ## 5 Conclusion

758

759 A first field CO_2-rich water leak experiment was carried out in a shallow freshwater
760 carbonate aquifer at the Saint-Emilion (France) pilot site in a limestone quarry. The addition
761 of $CO_{2\ (aq)}$ to the aquifer modified the initial calcocarbonic equilibrium of the carbonate
762 system. The decrease in pH, induced by the increase of $CO_{2\ (aq)}$ in the water, led to the
763 dissolution of carbonates and the contribution of ions in the aqueous phase, also evidenced by
764 the simultaneous increase in conductivity. The study of the chemical composition of the rock
765 showed that the trace elements were associated with calcite, quartz and iron oxides present in
766 smaller quantities. After the CO_2-rich-water injection, trace elements concentrations changed
767 according to six types of behavior. The release of these elements in the aqueous phase is often
768 strongly correlated with increasing alkalinity, presumably due to carbonate dissolution. As for
769 the major ions, the weaker increases of the trace element concentrations in the wells (except
770 for the injection well) were the result of the transport of the plume and the dilution from the
771 injection well. The small amount of carbonated water injected, combined with the buffering
772 capacity of the carbonate system, made it possible to limit the migration of trace elements to
773 the aqueous phase and highlight the rapid resilience of the carbonated system in these
774 injection conditions.

775 The geochemical impact of this experiment on the water quality of the aquifer was
776 minimal. Only As Ba, and Se exceeded the drinking water standards for a few hours.
777 Nevertheless, it is important to remember that the impact of a CO_2 leak will depend on the
778 volume of the aquifer, the composition of the rock, and the volume of CO_2 involved. Thus,

779 the results of this experiment provide answers to the behavior of a carbonate aquifer involved
780 in a potential CO_2 leak and supplement the data already present literature on this subject.
781 These data will be used for calibrating and validating geochemical models aimed at
782 determining the potential for mobilization of trace elements following a CO_2 leak in future
783 work.

784

785 ## 6 Declaration of interests

786

787 The authors declare that they have no known competing financial interests or personal
788 relationships that could have appeared to influence the work reported in this paper.

789 ## 7 Acknowledgments

790

791 This research was conducted within the Aquifer CO_2-Leak Project and we thank the
792 entire Aquifer CO_2-Leak Project team. This project is funded by the ADEME and the Région
793 Nouvelle Aquitaine, France. The authors are grateful to research G&E (EA 4592), Bordeaux
794 INP, and University Bordeaux Montaigne for creating a supportive and exciting research
795 environment. The authors are grateful to the laboratory EPOC (Talence, France) and more
796 particularly Alexandra Coynel, and Cécile Bossy from the M&M platform "Majeurs et
797 Métaux traces" to have permitted the analysis of several samples and to the ENSCBP
798 laboratory (Pessac, France) for the XRD analysis. The authors thank the reviewers for their
799 useful comments, their valuable time and their expertise.

800 ## 8 References

801

802 Aiuppa, A., Federico, C., Allard, P., Gurrieri, S., Valenza, M., 2005. Trace metal modeling of
803 groundwater–gas–rock interactions in a volcanic aquifer: Mount Vesuvius, Southern
804 Italy. Chem. Geol. 216, 289–311. https://doi.org/10.1016/j.chemgeo.2004.11.017
805 Alexandratos, V.G., Elzinga, E.J., Reeder, R.J., 2007. Arsenate uptake by calcite:
806 Macroscopic and spectroscopic characterization of adsorption and incorporation
807 mechanisms. Geochim. Cosmochim. Acta 71, 4172–4187.
808 https://doi.org/10.1016/j.gca.2007.06.055
809 Appelo, C.A.J., Postma, D., 2005. Geochemistry, groundwater and pollution, 2nd edition. ed.
810 CRC Press, Taylor & Francis Group, Boca Raton London New York.
811 Apps, J.A., Zheng, L., Spycher, N., Birkholzer, J.T., Kharaka, Y., Thordsen, J., Kakouros, E.,
812 Trautz, R., 2011. Transient changes in shallow groundwater chemistry during the
813 MSU ZERT CO2 injection experiment. Energy Procedia 4, 3231–3238.
814 https://doi.org/10.1016/j.egypro.2011.02.241
815 Auffray, B., 2014. Impact du stockage de CO_2 dans les systèmes réservoirs carbonatés :
816 interactions et transport d'éléments traces, effets sur les propriétés réservoirs (thesis).
817 http://www.theses.fr. Bordeaux 3.
818 Auffray, B., Garcia, B., Lienemann, C.-P., Sorbier, L., Cerepi, A., 2016. Zn(II), Mn(II) and
819 Sr(II) Behavior in a Natural Carbonate Reservoir System. Part I: Impact of Salinity,
820 Initial pH and Initial Zn(II) Concentration in Atmospheric Conditions. Oil Gas Sci.
821 Technol. – Rev. D'IFP Energ. Nouv. 71, 47. https://doi.org/10.2516/ogst/2015044
822 Aurelio, G., Fernández-Martínez, A., Cuello, G.J., Román-Ross, G., Alliot, I., Charlet, L.,
823 2010. Structural study of selenium(IV) substitutions in calcite. Chem. Geol. 270, 249–
824 256. https://doi.org/10.1016/j.chemgeo.2009.12.004
825 Ayers, R.S., Westcot, D.W., 1976. Water quality for agriculture, Irrigation and drainage
826 paper. Food and Agriculture Organization of the United Nations, Rome.

827 Bacci, G., Korre, A., Durucan, S., 2011. An experimental and numerical investigation into the
828 impact of dissolution/precipitation mechanisms on CO_2 injectivity in the wellbore and
829 far field regions. Int. J. Greenh. Gas Control 5, 579–588.
830 https://doi.org/10.1016/j.ijggc.2010.05.007
831 Bachu, S., 2008. CO_2 storage in geological media: Role, means, status and barriers to
832 deployment. Prog. Energy Combust. Sci. 34, 254–273.
833 https://doi.org/10.1016/j.pecs.2007.10.001
834 Bacon, D.H., Qafoku, N.P., Dai, Z., Keating, E.H., Brown, C.F., 2016. Modeling the impact
835 of carbon dioxide leakage into an unconfined, oxidizing carbonate aquifer. Int. J.
836 Greenh. Gas Control 44, 290–299. https://doi.org/10.1016/j.ijggc.2015.04.008
837 Bardelli, F., Benvenuti, M., Costagliola, P., Di Benedetto, F., Lattanzi, P., Meneghini, C.,
838 Romanelli, M., Valenzano, L., 2011. Arsenic uptake by natural calcite: An XAS study.
839 Geochim. Cosmochim. Acta 75, 3011–3023. https://doi.org/10.1016/j.gca.2011.03.003
840 Cahill, A.G., Jakobsen, R., 2013. Hydro-geochemical impact of CO_2 leakage from geological
841 storage on shallow potable aquifers: A field scale pilot experiment. Int. J. Greenh. Gas
842 Control 19, 678–688. https://doi.org/10.1016/j.ijggc.2013.03.015
843 Cahill, A.G., Jakobsen, R., Mathiesen, T.B., Jensen, C.K., 2013. Risks attributable to water
844 quality changes in shallow potable aquifers from geological carbon sequestration
845 leakage into sediments of variable carbonate content. Int. J. Greenh. Gas Control 19,
846 117–125. https://doi.org/10.1016/j.ijggc.2013.08.018
847 Cerepi, A., Humbert, L., Burlot, R., Pouchan, P., 1998. Détermination de la teneur en eau
848 d'un milieu poreux non saturé en utilisant Time Domain Reflectometry. Bull. Eng.
849 Geol. Environ. 57, 69–78. https://doi.org/10.1007/s100640050023
850 Cohen, G., Loisy, C., Laveuf, C., Le Roux, O., Delaplace, P., Magnier, C., Rouchon, V.,
851 Garcia, B., Cerepi, A., 2013. The CO_2-Vadose project: Experimental study and

modelling of CO_2 induced leakage and tracers associated in the carbonate vadose zone. Int. J. Greenh. Gas Control 14, 128–140. https://doi.org/10.1016/j.ijggc.2013.01.008

Comans, R.N.J., Middelburg, J.J., 1987. Sorption of trace metals on calcite: Applicability of the surface precipitation model. Geochim. Cosmochim. Acta 51, 2587–2591. https://doi.org/10.1016/0016-7037(87)90309-7

Damen, K., Faaij, A., Turkenburg, W., 2006. Health, Safety and Environmental Risks of Underground CO_2 Storage – Overview of Mechanisms and Current Knowledge. Clim. Change 74, 289–318. https://doi.org/10.1007/s10584-005-0425-9

Dickens, B., Bowen, J.S., 1971. The Crystal Structure of $BaCa(C0_3)_2$ (barytocalcite). J. Res. Natl. Bur. Stand., A. Physics and Chemistry 75A, 197–203.

Do, H.-K., Yun, S.-T., Yu, S., Ryuh, Y.-G., Choi, H.-S., 2020. Evaluation of Long-Term Impacts of CO2 Leakage on Groundwater Quality Using Hydrochemical Data from a Natural Analogue Site in South Korea. Water 12, 1457. https://doi.org/10.3390/w12051457

Dunham, R.R., 1962. Classification of Carbonate Rocks According to Depositional Texture in: Classification of Carbonate Rocks (W.E. Ham, Editor). Mem. Am. Assoc. Petrol. Geol. Pp. 183.

Farret, R., Thoraval, A., 2013. Retour d'expérience des incidents et accidents sur des sites d'exploitation ou de stockage en milieu souterrain – application au stockage géologique du CO_2.

Ford, D., Williams, P.W., 2007. Karst hydrogeology and geomorphology, Rev. ed. ed. John Wiley & Sons, Chichester, England ; a Hoboken, NJ.

Gal, F, Lions, J, Pokryszka, Z, Gombert, P, Grellier Solenne, Prevot, F, Darmoul, Y, Squarcioni, P, 2014. CO_2 leakage in a shallow aquifer – Observed changes in case of

small release. Energy Procedia 63, 4112–4122. https://doi.org/10.1016/j.egypro.2014.11.442

Gal, F., Proust, E., Humez, P., Braibant, G., Brach, M., Koch, F., Widory, D., Girard, J.-F., 2013. Inducing a CO_2 Leak into a Shallow Aquifer (CO_2FieldLab Eurogia+ Project): Monitoring the CO_2 Plume in Groundwaters. Energy Procedia 37, 3583–3593. https://doi.org/10.1016/j.egypro.2013.06.251

Gassara, O., Estublier, A., Garcia, B., Noirez, S., Cerepi, A., Loisy, C., Le Roux, O., Petit, A., Rossi, L., Kennedy, S., Brichart, T., Chiquet, P., Luu Van Lang, L., André Duboin, F., Gance, J., Texier, B., Lavielle, B., Thomas, B., 2021. The Aquifer-CO_2Leak project: Numerical modeling for the design of a CO_2 injection experiment in the saturated zone of the Saint-Emilion (France) site. Int. J. Greenh. Gas Control 104, 103196. https://doi.org/10.1016/j.ijggc.2020.103196

Gheno, T., Monceau, D., Young, D.J., 2012. Mechanism of breakaway oxidation of Fe–Cr and Fe–Cr–Ni alloys in dry and wet carbon dioxide. Corros. Sci. S0010938X12003538. https://doi.org/10.1016/j.corsci.2012.07.024

Giese, R., Henninges, J., Lüth, S., Morozova, D., Schmidt-Hattenberger, C., Würdemann, H., Zimmer, M., Cosma, C., Juhlin, C., 2009. Monitoring at the CO_2 SINK site: A concept integrating geophysics, geochemistry and microbiology. Energy Procedia 1, 2251–2259. https://doi.org/10.1016/j.egypro.2009.01.293

Gil-Díaz, T., Schäfer, J., Coynel, A., Bossy, C., Dutruch, L., Blanc, G., 2018. Antimony in the Lot–Garonne river system: a 14-year record of solid–liquid partitioning and fluxes. Environ. Chem. 15, 121. https://doi.org/10.1071/EN17188

Golding, S.D., Uysal, I.T., Boreham, C.J., Kirste, D., Baublys, K.A., Esterle, J.S., 2011. Adsorption and mineral trapping dominate CO_2 storage in coal systems. Energy Procedia 4, 3131–3138. https://doi.org/10.1016/j.egypro.2011.02.227

Graf, D.L., 1962. Minor element distribution in sedimentary carbonate rocks. Geochim. Cosmochim. Acta 26, 849–856.

Gunter, W.D., Bachu, S., Benson, S., 2004. The role of hydrogeological and geochemical trapping in sedimentary basins for secure geological storage of carbon dioxide. Geol. Soc. Lond. Spec. Publ. 233, 129–145. https://doi.org/10.1144/GSL.SP.2004.233.01.09

Harvey, O.R., Qafoku, N.P., Cantrell, K.J., Lee, G., Amonette, J.E., Brown, C.F., 2012. Geochemical Implications of Gas Leakage associated with Geologic CO_2 Storage—A Qualitative Review. https://doi.org/10.1021/es3029457

Humez, P., Lagneau, V., Lions, J., Negrel, P., 2013. Assessing the potential consequences of CO2 leakage to freshwater resources: A batch-reaction experiment towards an isotopic tracing tool. Appl. Geochem. 30, 178–190. https://doi.org/10.1016/j.apgeochem.2012.07.014

INERIS, 2018. Synthèse des valeurs réglementaires pour les substances chimiques, en vigueur dans l'eau, les denrées alimentaires et dans l'air (No. INERIS-DRC-17-164559-10404A).

IPCC, 2005. IPCC special report on carbon dioxide capture and storage. Cambridge University Press, for the Intergovernmental Panel on Climate Change, Cambridge.

Jones, D.G., Beaubien, S.E., Blackford, J.C., Foekema, E.M., Lions, J., De Vittor, C., West, J.M., Widdicombe, S., Hauton, C., Queirós, A.M., 2015. Developments since 2005 in understanding potential environmental impacts of CO_2 leakage from geological storage. Int. J. Greenh. Gas Control 40, 350–377. https://doi.org/10.1016/j.ijggc.2015.05.032

Keating, E.H., Fessenden, J., Kanjorski, N., Koning, D.J., Pawar, R., 2010. The impact of CO_2 on shallow groundwater chemistry: observations at a natural analog site and

implications for carbon sequestration. Environ. Earth Sci. 60, 521–536. https://doi.org/10.1007/s12665-009-0192-4

Kharaka, Y.K., Thordsen, J.J., Kakouros, E., Ambats, G., Herkelrath, W.N., Beers, S.R., Birkholzer, J.T., Apps, J.A., Spycher, N.F., Zheng, L., Trautz, R.C., Rauch, H.W., Gullickson, K.S., 2010. Changes in the chemistry of shallow groundwater related to the 2008 injection of CO_2 at the ZERT field site, Bozeman, Montana. Environ. Earth Sci. 60, 273–284. https://doi.org/10.1007/s12665-009-0401-1

Lawter, A.R., Qafoku, N.P., Asmussen, R.M., Kukkadapu, R.K., Qafoku, O., Bacon, D.H., Brown, C.F., 2018. Element mobilization and immobilization from carbonate rocks between CO_2 storage reservoirs and the overlying aquifers during a potential CO2 leakage. Chemosphere 197, 399–410. https://doi.org/10.1016/j.chemosphere.2017.12.199

Lemieux, J.-M., 2011. Review: The potential impact of underground geological storage of carbon dioxide in deep saline aquifers on shallow groundwater resources. Hydrogeol. J. 19, 757–778. https://doi.org/10.1007/s10040-011-0715-4

Lions, J., Devau, N., de Lary, L., Dupraz, S., Parmentier, M., Gombert, P., Dictor, M.-C., 2014. Potential impacts of leakage from CO_2 geological storage on geochemical processes controlling fresh groundwater quality: A review. Int. J. Greenh. Gas Control 22, 165–175. https://doi.org/10.1016/j.ijggc.2013.12.019

Little, M.G., Jackson, R.B., 2010. Potential Impacts of Leakage from Deep CO_2 Geosequestration on Overlying Freshwater Aquifers. Environ. Sci. Technol. 44, 9225–9232. https://doi.org/10.1021/es102235w

Loisy, C., Cohen, G., Laveuf, C., Le Roux, O., Delaplace, P., Magnier, C., Rouchon, V., Cerepi, A., Garcia, B., 2013. The CO_2-Vadose Project: Dynamics of the natural CO_2

in a carbonate vadose zone. Int. J. Greenh. Gas Control 14, 97–112. https://doi.org/10.1016/j.ijggc.2012.12.017

Lu, J., Kharaka, Y.K., Thordsen, J.J., Horita, J., Karamalidis, A., Griffith, C., Hakala, J.A., Ambats, G., Cole, D.R., Phelps, T.J., Manning, M.A., Cook, P.J., Hovorka, S.D., 2012. CO_2–rock–brine interactions in Lower Tuscaloosa Formation at Cranfield CO_2 sequestration site, Mississippi, U.S.A. Chem. Geol. 291, 269–277. https://doi.org/10.1016/j.chemgeo.2011.10.020

Marshall, C.P., Fairbridge, R.W., 1999. Encyclopedia of geochemistry, Kluwer Academic encyclopedia of earth sciences series. Kluwer Academic Publishers, Dordrecht ; Boston.

Montes-Hernandez, G., Renard, F., Lafay, R., 2013. Experimental Assessment of CO_2 - Mineral-Toxic Ion Interactions in a Simplified Freshwater Aquifer: Implications for CO_2 Leakage from Deep Geological Storage. Environ. Sci. Technol. 47, 6247–6253. https://doi.org/10.1021/es3053448

Ni, S., Ju, Y., Hou, Q., Wang, S., Liu, Q., Wu, Y., Xiao, L., 2009. Enrichment of heavy metal elements and their adsorption on iron oxides during carbonate rock weathering process. Prog. Nat. Sci. 19, 1133–1139. https://doi.org/10.1016/j.pnsc.2009.01.008

Petit, A., Cerepi, A., Loisy, C., Le Roux, O., Rossi, L., Estublier, A., Gance, J., Garcia, B., Hautefeuille, B., Lavielle, B., Brichart, T., Noirez, S., Martin, F., Texier, B., Kennedy, S., EL Khamlichi, A., 2021. Aquifer-CO_2 leak project: Physicochemical characterization of the CO_2 leakage impact on a carbonate shallow freshwater aquifer. Int. J. Greenh. Gas Control 106, 103231. https://doi.org/10.1016/j.ijggc.2020.103231

Pingitore, N.E., Eastman, M.P., 1986. The coprecipitation of Sr2+ with calcite at 25°C and 1 atm. Geochim. Cosmochim. Acta 50, 2195–2203. https://doi.org/10.1016/0016-7037(86)90074-8

975 Qafoku, N.P., Lawter, A.R., Bacon, D.H., Zheng, L., Kyle, J., Brown, C.F., 2017. Review of
976 the impacts of leaking CO_2 gas and brine on groundwater quality. Earth-Sci. Rev. 169,
977 69–84. https://doi.org/10.1016/j.earscirev.2017.04.010
978 Reeder, R.J., Lamble, G.M., Lee, J.-F., Staudt, W.J., 1994. Mechanism of SeO_4^{2-} substitution
979 in calcite: An XAFS study. Geochim. Cosmochim. Acta 58, 5639–5646.
980 https://doi.org/10.1016/0016-7037(94)90256-9
981 Rhino, K., Loisy, C., Cerepi, A., Le roux, O., Garcia, B., Rouchon, V., Noirez, S., Le Gallo,
982 C., Delaplace, P., Willequet, O., Bertrand, C., Khamlichi, A.E., 2016. The Demo-CO_2
983 project: Monitoring and comparison of two shallow subsurface CO_2 leakage
984 experiments with gas tracer associated in the carbonate vadose zone. Int. J. Greenh.
985 Gas Control 53, 207–221. https://doi.org/10.1016/j.ijggc.2016.07.032
986 Rillard, J., Gombert, P., Toulhoat, P., Zuddas, P., 2014. Geochemical assessment of CO_2
987 perturbation in a shallow aquifer evaluated by a push–pull field experiment. Int. J.
988 Greenh. Gas Control 21, 23–32. https://doi.org/10.1016/j.ijggc.2013.11.019
989 Rillard, J., Loisy, C., Le Roux, O., Cerepi, A., Garcia, B., Noirez, S., Rouchon, V., Delaplace,
990 P., Willequet, O., Bertrand, C., 2015. The DEMO-CO_2 project: A vadose zone CO_2
991 and tracer leakage field experiment. Int. J. Greenh. Gas Control 39, 302–317.
992 https://doi.org/10.1016/j.ijggc.2015.04.012
993 Ringrose, P., Atbi, M., Mason, D., Espinassous, M., Myhrer, O., Iding, M., Mathieson, A.,
994 Wright, I., 2009. Plume development around well KB-502 at the In Salah CO2 storage
995 site. First Break Spetial Top. Volume 27, 85–89.
996 Rouff, A.A., Elzinga, E.J., Reeder, R.J., Fisher, N.S., 2004. X-ray Absorption Spectroscopic
997 Evidence for the Formation of Pb(II) Inner-Sphere Adsorption Complexes and
998 Precipitates at the Calcite−Water Interface. Environ. Sci. Technol. 38, 1700–1707.
999 https://doi.org/10.1021/es0345625

1000 Saito, A., Kagi, H., Marugata, S., Komatsu, K., Enomoto, D., Maruyama, K., Kawano, J.,
1001 2020. Incorporation of Incompatible Strontium and Barium Ions into Calcite ($CaCO_3$)
1002 through Amorphous Calcium Carbonate. Minerals 10, 270.
1003 https://doi.org/10.3390/min10030270
1004 Shao, H., Freiburg, J.T., Berger, P.M., Taylor, A.H., Cohen, H.F., Locke, R.A., 2020.
1005 Mobilization of trace metals from caprock and formation rocks at the Illinois Basin –
1006 Decatur Project demonstration site under geological carbon dioxide sequestration
1007 conditions. Chem. Geol. 550, 119758. https://doi.org/10.1016/j.chemgeo.2020.119758
1008 Smith, D.I., Mead, D.G., 1962. The Solution of Limestone, With special Rreference to
1009 Mendip, in: Proc. Univ. Bristol Speleological Soc., 9. pp. 188–211.
1010 Tambach, T., Koenen, M., van Bergen, F., 2011. Geochemical evaluation of CO_2 injection
1011 into storage reservoirs based on case-studies in the Netherlands. Energy Procedia 4,
1012 4747–4753. https://doi.org/10.1016/j.egypro.2011.02.438
1013 Tanji, K., Valoppi, L., 1989. Groundwater contamination by trace elements. Agric. Ecosyst.
1014 Environ. 26, 229–274. https://doi.org/10.1016/0167-8809(89)90015-7
1015 Thompson, G., Bankston, D.C., Pasley, S.M., 1970. Trace element data for reference
1016 carbonate rocks. Chem. Geol. 6, 165–170. https://doi.org/10.1016/0009-
1017 2541(70)90015-X
1018 Thorstenson, D.C., Plummer, L.N., 1977. Equilibrium criteria for two-component solids
1019 reacting with fixed composition in an aqueous phase; example, the magnesian calcites.
1020 Am. J. Sci. 277, 1203–1223. https://doi.org/10.2475/ajs.277.9.1203
1021 Trautz, R.C., Pugh, J.D., Varadharajan, C., Zheng, L., Bianchi, M., Nico, P.S., Spycher, N.F.,
1022 Newell, D.L., Esposito, R.A., Wu, Y., Dafflon, B., Hubbard, S.S., Birkholzer, J.T.,
1023 2013. Effect of Dissolved CO_2 on a Shallow Groundwater System: A Controlled

1024 Release Field Experiment. Environ. Sci. Technol. 47, 298–305.
1025 https://doi.org/10.1021/es301280t
1026 USGS, 2012. Alkalinity and Acid Neutralizing Capacity, in: U.S. Geological Survey TWRI
1027 Book 9 Chapter A6. p. 45.
1028 Vincent, M., Maton, C., 1999. Caractérisation de l'aléa lié à la présence de carrières
1029 souterraines abandonnées en périphérie immédiate de la ville de Saint-Emilion
1030 (Gironde). Rapport BRGM, R40635.
1031 Vouvé, M., 1990. Eglise monolithe de Saint-Emilion. Etude du contexte géologique et des
1032 désordres géomécaniques. . Centre d'Hydrogéologie. Université de Bordeaux 1, CH
1033 90120, 206 p., 3 tome.
1034 Wang, G., Qafoku, N.P., Lawter, A.R., Bowden, M., Harvey, O., Sullivan, C., Brown, C.F.,
1035 2016. Geochemical impacts of leaking CO_2 from subsurface storage reservoirs to an
1036 unconfined oxidizing carbonate aquifer. Int. J. Greenh. Gas Control 44, 310–322.
1037 https://doi.org/10.1016/j.ijggc.2015.07.002
1038 WHO, 2017. Guidelines for drinking-water quality, 4th edition, incorporating the 1st
1039 addendum.
1040 Wilkinson, M., Carruthers, K., Thomas, A.L., Haszeldine, R.S., 2020. The performance of
1041 leaching experiments to assess the potential mobilization of trace elements during CO_2
1042 injection. Appl. Geochem. 120, 104667.
1043 https://doi.org/10.1016/j.apgeochem.2020.104667
1044 Wunsch, A., Navarre-Sitchler, A.K., Moore, J., McCray, J.E., 2014. Metal release from
1045 limestones at high partial-pressures of CO2. Chem. Geol. 363, 40–55.
1046 https://doi.org/10.1016/j.chemgeo.2013.10.036
1047 Yang, C., Mickler, P.J., Reedy, R., Scanlon, B.R., Romanak, K.D., Nicot, J.-P., Hovorka,
1048 S.D., Trevino, R.H., Larson, T., 2013. Single-well push–pull test for assessing

potential impacts of CO_2 leakage on groundwater quality in a shallow Gulf Coast aquifer in Cranfield, Mississippi. Int. J. Greenh. Gas Control 18, 375–387. https://doi.org/10.1016/j.ijggc.2012.12.030

Zachara, J.M., Cowan, C.E., Resch, C.T., 1991. Sorption of divalent metals on calcite. Geochim. Cosmochim. Acta 55, 1549–1562. https://doi.org/10.1016/0016-7037(91)90127-Q

Zevenhoven, R., Eloneva, S., Teir, S., 2006. Chemical fixation of CO2 in carbonates: Routes to valuable products and long-term storage. Catal. Today 115, 73–79. https://doi.org/10.1016/j.cattod.2006.02.020

Zheng, L., Spycher, N., Bianchi, M., Pugh, J.D., Varadharajan, C., Tinnacher, R.M., Birkholzer, J.T., Nico, P., Trautz, R.C., 2016. Impacts of elevated dissolved CO_2 on a shallow groundwater system: Reactive transport modeling of a controlled-release field test. Chem. Geol. 447, 117–132. https://doi.org/10.1016/j.chemgeo.2016.10.027

Zheng, L., Spycher, N., Varadharajan, C., Tinnacher, R.M., Pugh, J.D., Bianchi, M., Birkholzer, J., Nico, P.S., Trautz, R.C., 2015. On the mobilization of metals by CO_2 leakage into shallow aquifers: exploring release mechanisms by modeling field and laboratory experiments. Greenh. Gases Sci. Technol. 5, 403–418. https://doi.org/10.1002/ghg.1493

Zhu, Q., Li, X., Jiang, Z., Wei, N., 2015. Impacts of CO2 leakage into shallow formations on groundwater chemistry. Fuel Process. Technol. 135, 162–167. https://doi.org/10.1016/j.fuproc.2014.11.042

1074

1075 **Figures, tables, and their captions**

1076 **Figure 1 (Color should be used in print)**

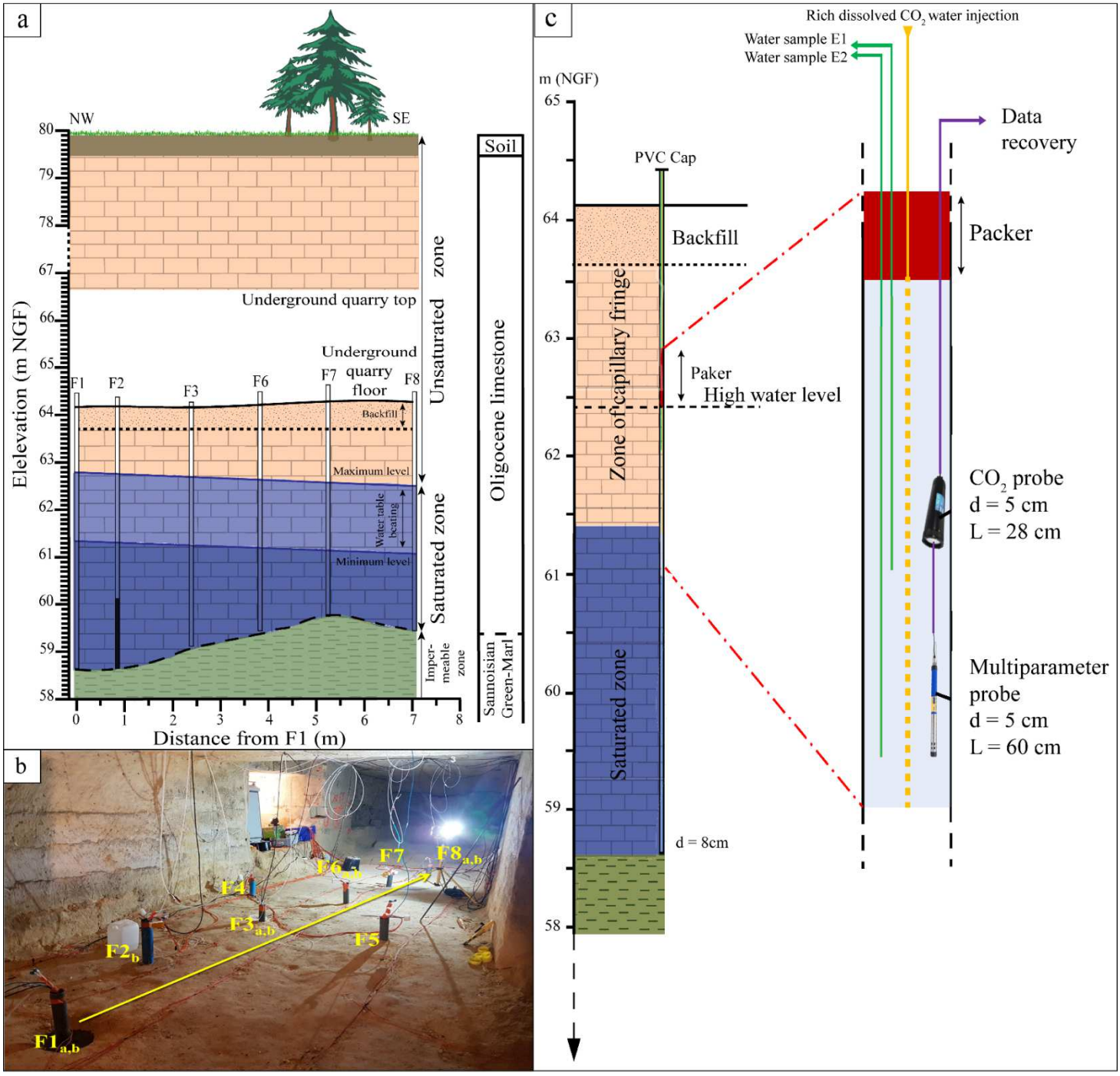

1077

1078

Fig.1: Configuration of the experimental site in the underground quarry **a:** Cross-section in the Upper 1b Oligocene limestone. The quarry floor is located approximately 16m from the surface. The water table is beaten over 1.40 m with a maximal hydraulic gradient of 5% and an NW-SE direction. The mean of the hydraulic gradient is 2% for this experiment and corresponds to the moment when the water table rise was 61.35 m NGF. Sannoisian green marls are visible around 59m NGF on average. The boreholes used for the experiment go through a part of the unsaturated zone and the saturated zone. **b:** Top view of the 8 boreholes (F1 to F8) on the quarry floor in the experimental zone. They are arranged along an axis parallel to the hydraulic gradient. The yellow arrow indicates the direction of the groundwater flow and the direction of propagation of the CO_2-rich water plume during the experiment. The index "a" near the borehole head indicates that the well is equipped with a multi-parameter probe. The index "b" indicates that the well is equipped with a CO_2 probe. F1 is the injection well. Samples of water were taken throughout the experiment in all boreholes and at two elevations. **c:** Example of configuration of well F1. The multiparameter probe, the CO_2 probe, and the sampling tubing are located below a packer. Samples were taken at depth E1 (25 cm) and E2 (70 cm) (respectively 61.10 m NGF, and 60.65 m NGF for the well F1).

1102 **Figure 2 (Color should be used in print)**

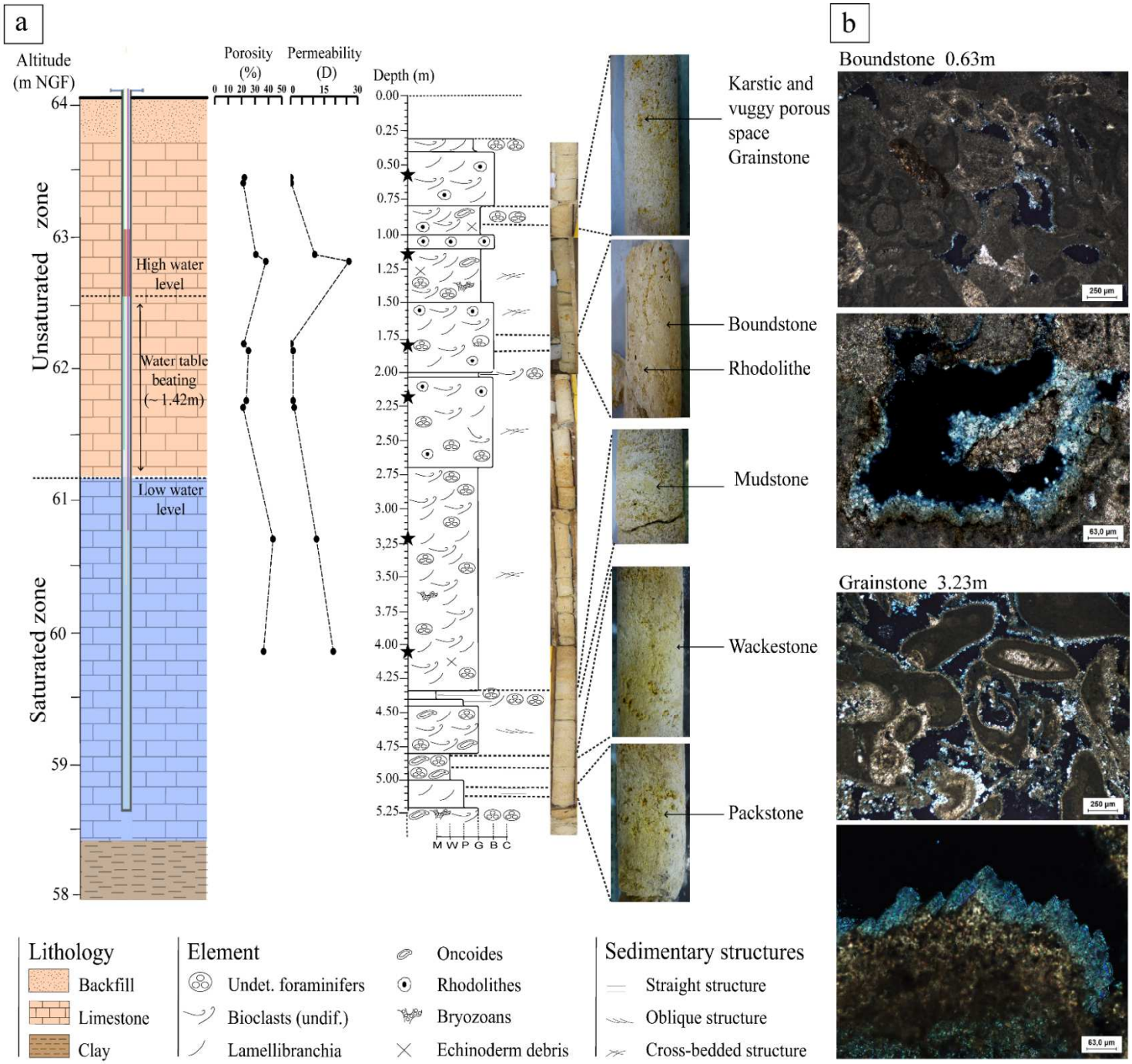

1103

1104 **Fig.2**: Physical characterization of the Oligocene limestone (Petit et al., 2021, modified). **a:**
1105 Cross-section of well F2: From right to left, the drawing shows (1) the hydrogeologic context
1106 with the maximum and minimum level of the water table beating, the thickness of the
1107 limestone layer, and the start of clay formation; (2) the evolution of porosity (%) measured by

Hg-injection; (3) the evolution of permeability (D) measured by variable head air permeameter methods respectively. The porosity and the permeability were measured at a different level from 63.5 m to 59.5 m NGF, throughout the capillary fringe and saturated zone; (4) the stratigraphic log and associated macroscopic facies. Black stars represent the places in the sediment core where samples were collected at 0.63, 1.15, 1.80, 2.22, 3.23 and 4.05 meters from the quarry floor (67.17m NGF). Total trace metal element concentrations were measured on these six limestone samples (**Tab.2**). The facies represented are for the most part grainstone and boundstone. **b:** Microscope photograph of the limestone: boundstone has been collected at 0.63 meters from the quarry floor and the grainstone at 3.23 m. These views highlight the porosity difference between the two facies. They also highlight the larger share of recrystallized space in the pores of the grainstone.

Figure 3 (Color should be used in print)

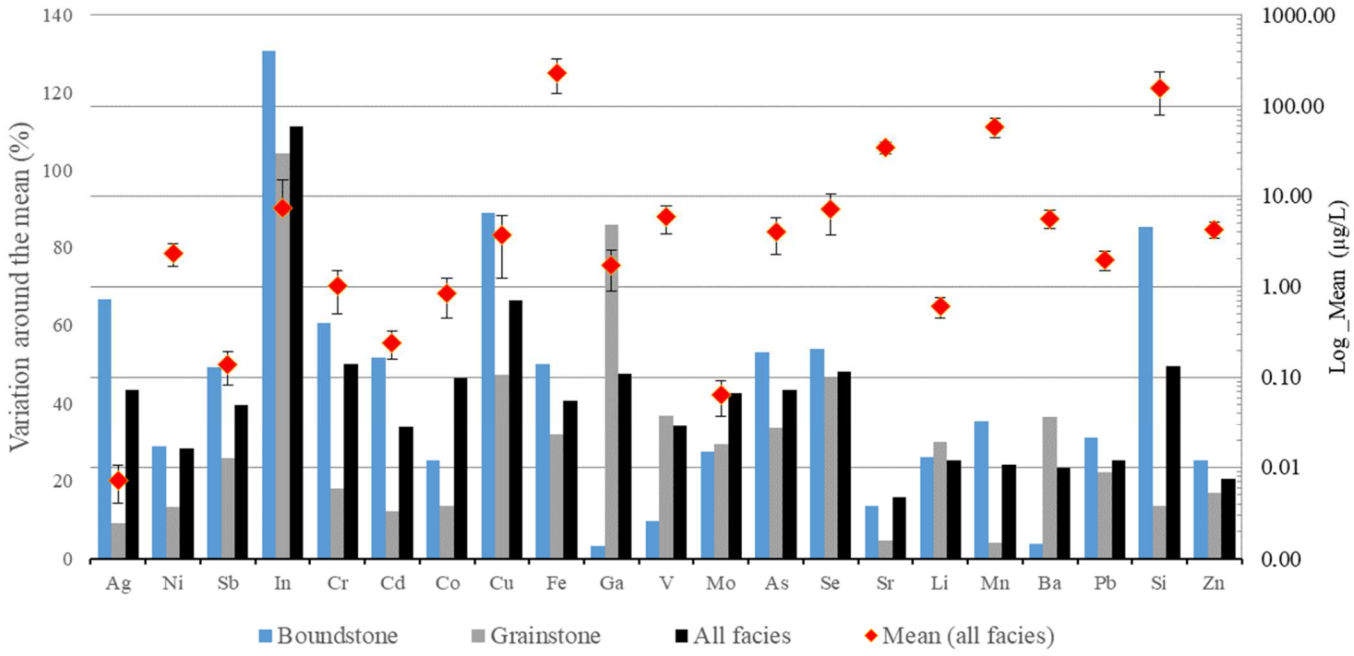

Fig.3: Variation of the concentrations around the mean in percent (i.e. standard deviation in percent) for each trace ion analyzed in the 6 carbonate rock samples taken from the F2 core. Blue bars represent the degree of percent variation around the mean in three boundstone samples. Grey bars represent the degree of percent variation around the mean in three grainstone samples. The black bars correspond to the degree of variation around the mean of the concentrations of each trace elements of the six samples. The mean concentrations of the six samples (± standard deviation) of each element are represented by the red diamonds (µg/L). The secondary vertical axis is expressed in log.

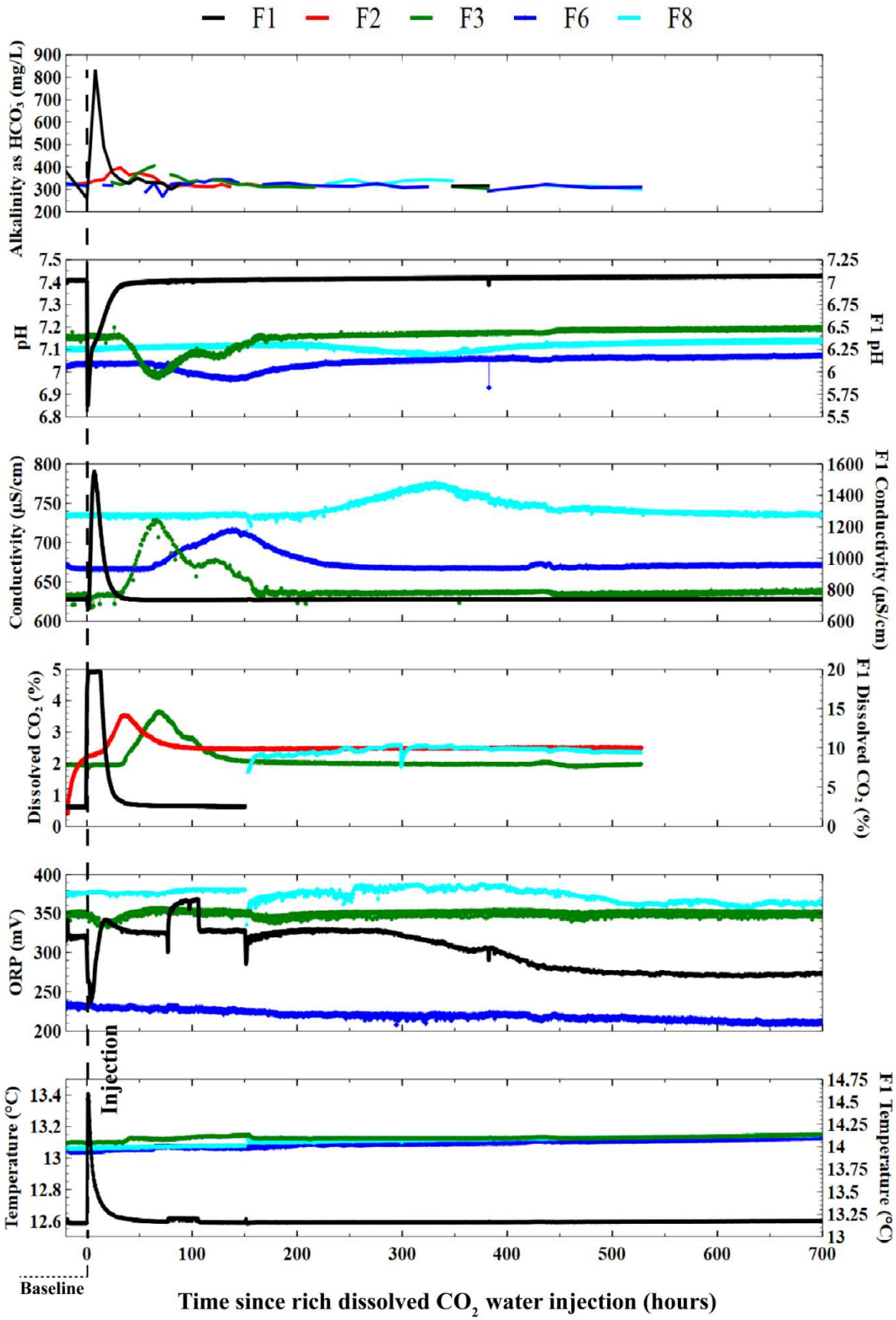

1142 **Figure 4 (Color should be used in print)**

Fig.4: Evolution and comparison of the different physic-geochemical parameters measured in wells F1, F2, F3, F6, and F8. The parameters were obtained using multiparameter probes (temperature (±0.1°C); ORP (±5.0 mV at 25°C); conductivity (± 0.5% of reading plus 1 µS/cm from 0 to 100.000 µS/cm) and pH (±0.1 pH units or better) and CO_2 probes (pCO_2 10-900 mbar ± 10%). Well F2 is only equipped with a CO_2 probe. Alkalinity (as HCO_3^- ; mg/L) were measured in the laboratory by the Inflection Point Titration Method. The injection started at t=0 and lasting 1.5 hours. For a better visibility, data for the conductivity, dissolved CO_2, and pH from well F1 have been added on a second y-axis on the right of the graph. The CO_2 probe initially installed in well F1 was moved to well F8 from 145 hours after the plume of CO_2 had dissipated in F1. Therefore, there are no data for the F8 well before 145h. The sudden decrease occurring at this time corresponds to the withdrawal and re-filling of the probe.

1165

1166 **Figure 5 (Color should be used in print)**

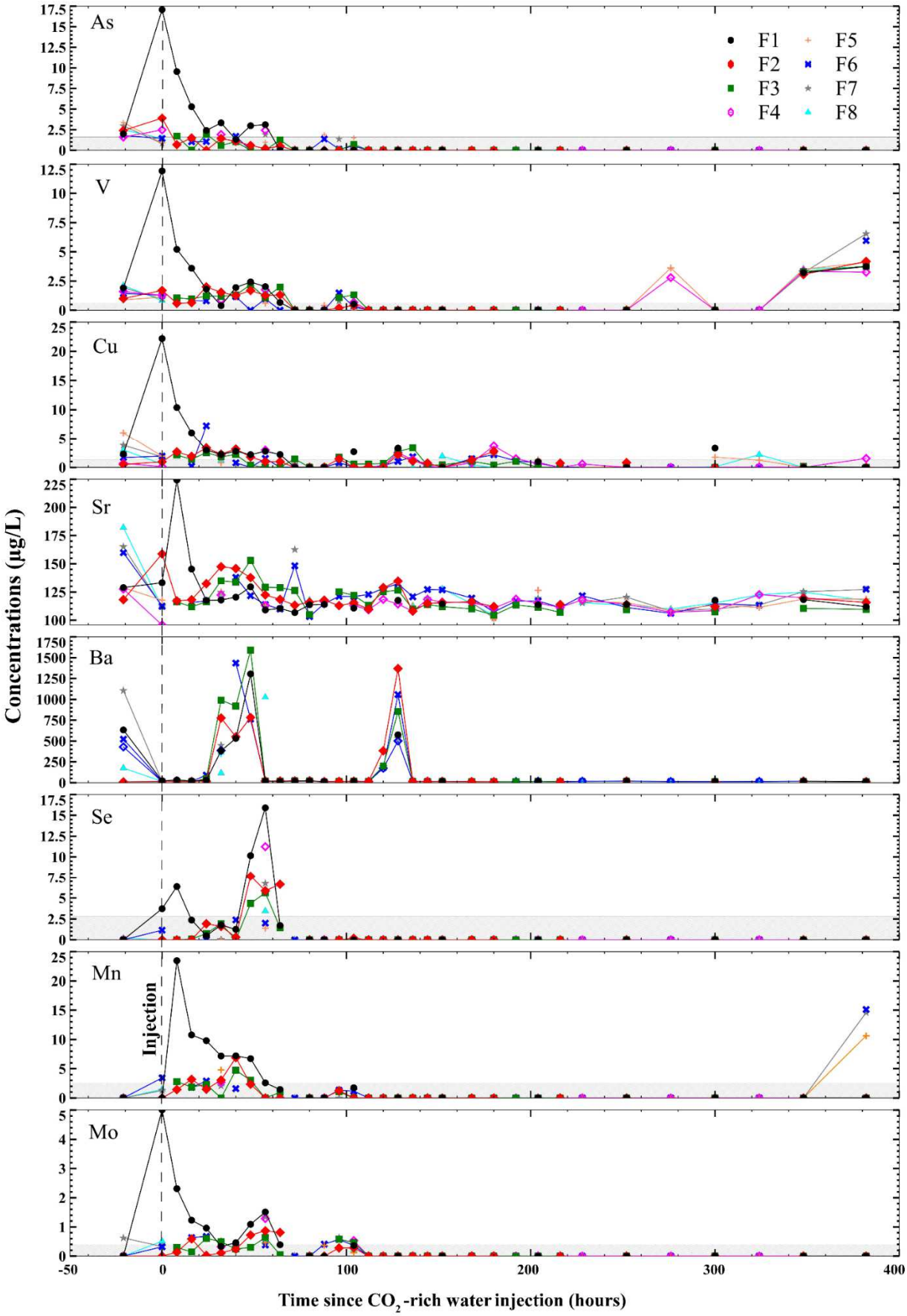

Fig.5: Evolution of As, V, Cu, Sr, Ba, Se, Mn, and Mo concentrations of the wells F1, F2, F3, F4, F5, F6, F7 and F8 in the function of time since CO_2–rich water injection. Concentrations units are in µg/L. The axis F1 to F8 is parallel to the flow direction of the aquifer (Fig.1). Waters samples were collected at 25 cm under the water table (i.e. 61.10 m NGF for the well F1). The hatched area highlights samples under the detection limit. The injection started at t=0.

1189

1190 **Figure 6 (Color should be used in print)**

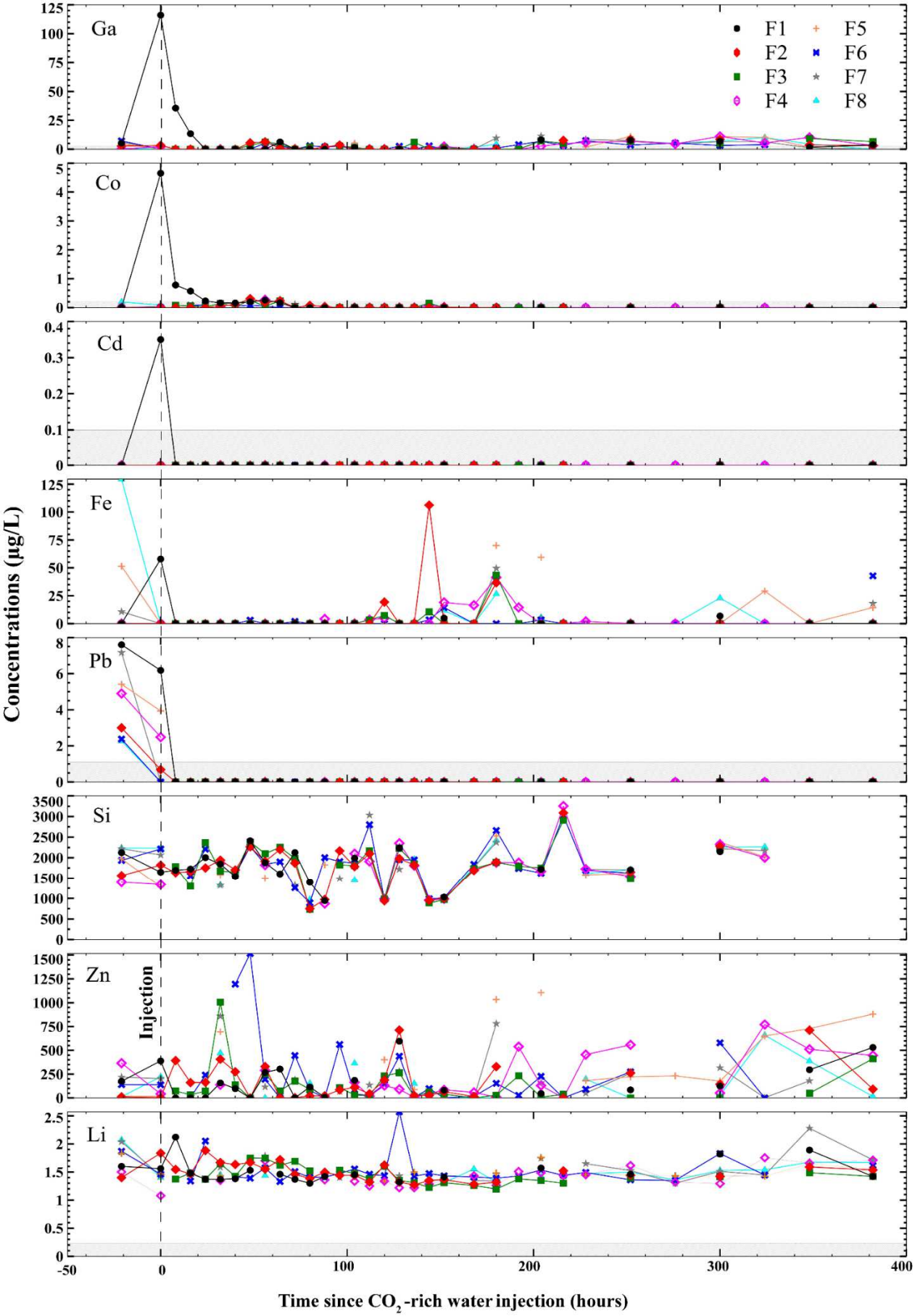

Fig.6: Evolution of Ga, Co, Cd, Fe, Pb, Si, Zn and Li concentrations of the wells F1, F2, F3, F4, F5, F6, F7 and F8 in the function of time since CO_2 -rich water injection. Concentrations units are in µg/L. The axis F1-F2-F3-F6-F7-F8 is parallel to the flow direction of the aquifer. The axis F3-F4-F5 is perpendicular to the flow direction of the aquifer. Waters samples were collected at 25 cm under the water table (i.e. 61.10 m NGF for the well F1). The hatched area highlights samples under the detection limit. The injection started at t=0.

Figure 7 (Color should be used in print)

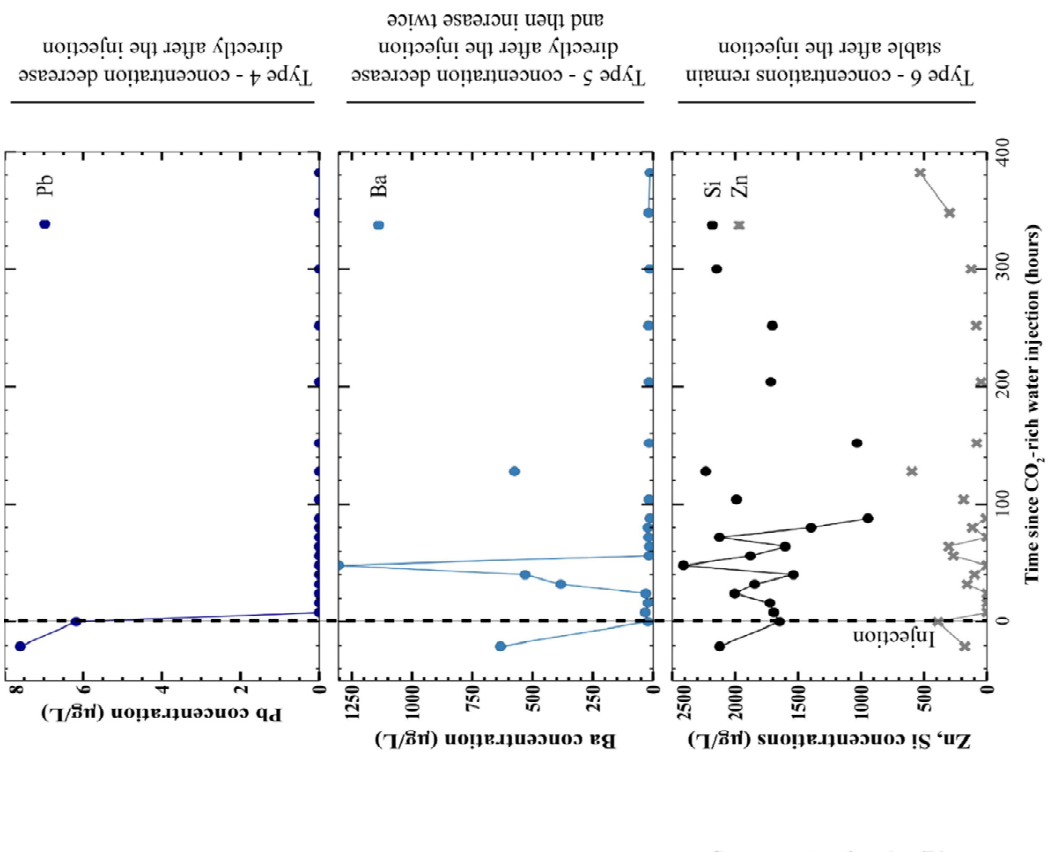

Fig.7: Evolution of the trace element concentrations of the well F1 function of time since injection (µg/L). The data presented correspond to the concentrations at depth E1 (25cm) under the water table (i.e. 61.15 m NGF). The injection started at t=0. Elements have been grouped into six types according to their behavior following the injection of CO_2-rich water.

Figure 8 (Color should be used in print)

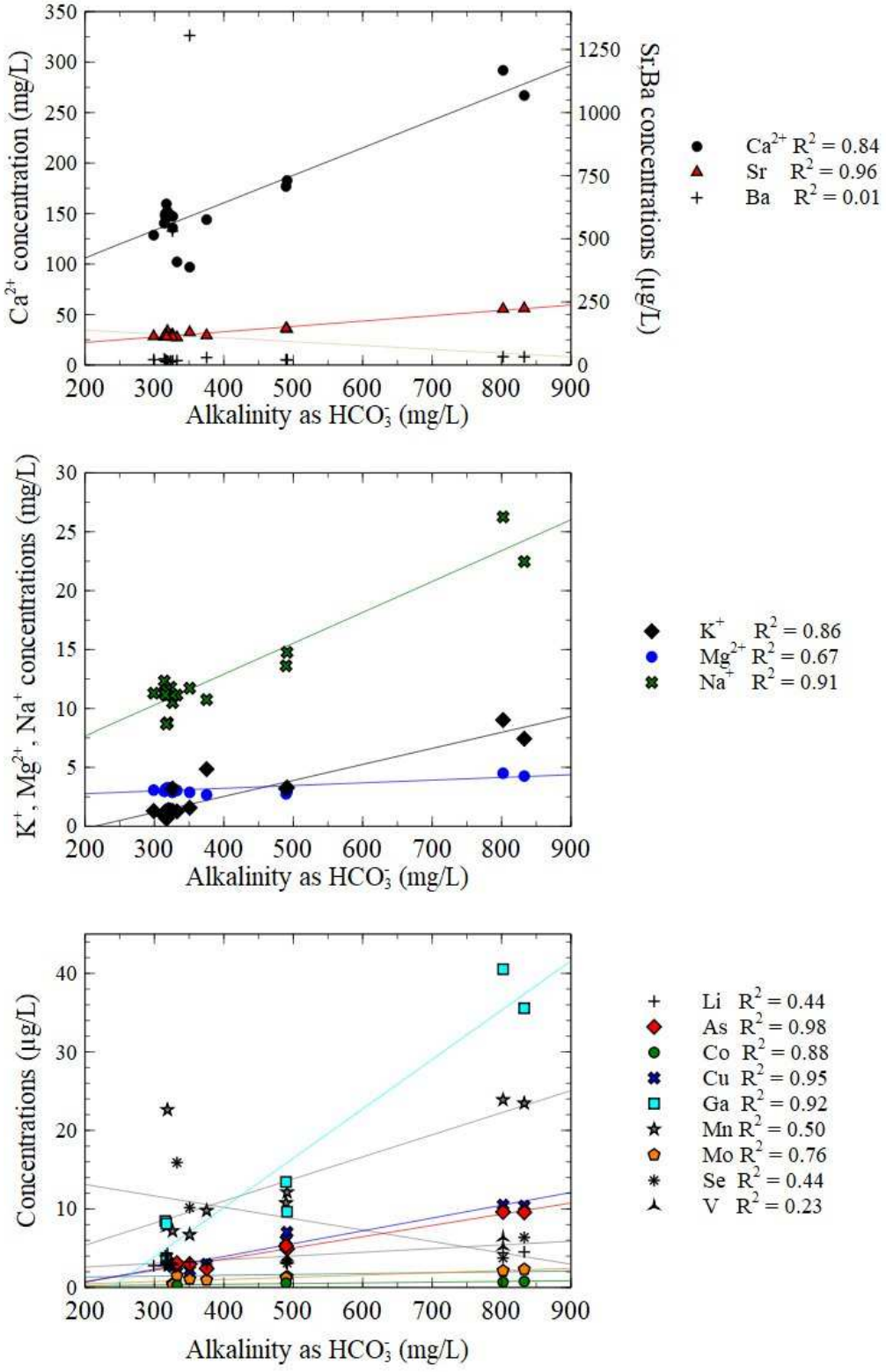

Fig.8: Relation between the alkalinity represented by the HCO_3^- concentrations and the different cations and trace elements analyzed. The concentrations of the cations K^+, Na^+, Ca^{2+} are given in mg/L and the concentrations of the trace elements are in µg/L. The coefficient of determination (R^2) has been added to the graph for each element.

Figure 9 (Color should be used in print)

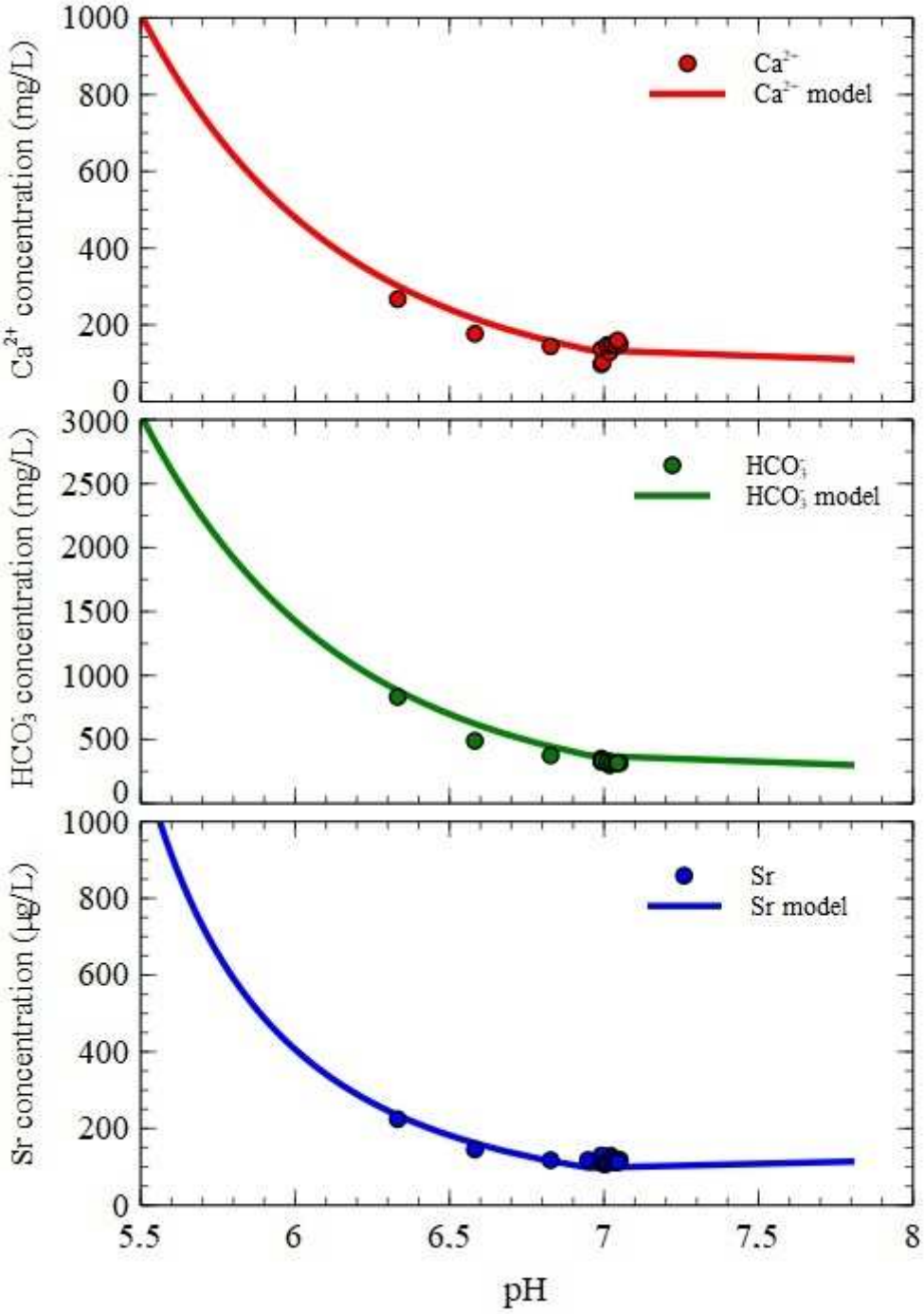

Fig.9: Concentrations of Ca^{2+}, HCO_3^- and Sr as function of pH. The points correspond to the experimental data. The curve corresponds to the results of the carbonate dissolution model performed using PhreeqC.

1266 # Table 1

1267 **Tab.1**: Characteristics of the injection experiment: physicochemical parameters of the rich

1268 dissolved-CO_2-water injected and injection conditions.

Physicochemical parameters of the injected water	
Composition of the gas used for gasified	90% CO_2 + 9% He + 1% Kr
Gasified water volume (L)	200
pH	5.45
Conductivity (µS/cm)	645
Injection conditions	
Injection velocity (L/min)	2.2
Injection duration (hours)	1.5
Velocity of the groundwater (m/day)	0.8

1269

1270 # Table 2

1271 **Tab.2:** Elemental composition of the 6 samples of limestone analyzed using X-ray

1272 fluorescence (XRF). Values represent the mean of six punctual random analyses on a circle of

1273 100 µm in diameter, on each powder samples. Results are semi-quantitative and in percent

1274 (%). The symbol ND means that the element was not detected by the machine. The grey

1275 columns underline the most represented elements.

	Mass (%)	**Al**	**Si**	**S**	**K**	**Ca**	**V**	**Ti**	**Mn**	**Fe**	**Cu**	**Sr**	**Zn**	**Pt**	**Ba**
Boundstone	**F2_0.63**	0.50	4.04	0.01	0.14	94.04	ND	0.09	0.09	1.10	ND	ND	ND	ND	ND
	F2_1.80	18.96	13.35	0.01	2.87	62.02	0.01	0.22	0.01	2.37	0.02	ND	0.01	0.05	0.10
	F2_2.22	ND	3.42	0.01	0.02	95.68	ND	ND	0.02	0.86	ND	ND	ND	ND	ND
Grainstone	**F2_3.23**	ND	3.14	0.50	ND	92.11	ND	ND	2.23	1.22	0.81	ND	ND	ND	ND
	F2_4.05	2.99	8.17	0.03	1.41	83.51	ND	0.06	0.24	3.59	ND	ND	ND	ND	ND
	F2_1.15	2.04	25.09	ND	2.74	69.56	0.04	0.05	0.06	0.34	0.00	0.03	ND	ND	ND

1276

1277

Table 3

Tab.3: Mean of the total trace elements concentrations contained in our six limestone samples collected during the F2 drilling (mg/Kg). Average concentrations were also calculated for each facies (3 samples per facies). After tri-acid digestion with HCl, HNO_3, and HF, concentrations of Ag, As, Ba, Cd, Co, Cr, Cu, Mo, Ni, Pb, Sb, Sr, V and Zn were obtained using an ICP-MS (EPOC Laboratory, France) while Be, Fe, Ga, Li, Mn, In, Se and Si were obtained using an ICP-AES (ENSEGID, France) on a representative aliquot of rocks samples (i.e. 150 mg of each samples). Sd means standard deviation. Values on the right are results come from Baptiste Auffray's (2014) thesis work on carbonates rocks come from Saint-Emilion quarry too and Lavoux carbonates samples. The <LD symbol is used to denote a value under the detection limit. The ND symbol indicates no data. Values on the left are the maximums concentrations of dissolved trace elements in the injection well F1.

(µg/L)	*Maximum concentration of $ETM_{dissolved}$ in the aqueous phase (Well F1)*	**Mean concentration on six limestone samples (this study) (mg/Kg)**		**Mean concentration on bounstone samples (this study) (mg/Kg)**		**Mean concentration on grainstone samples (this study) (mg/Kg)**		**Limestone samples *(Auffray. 2014)* (mg/Kg)**	
		(n=6)	***Sd***	***(n=3)***	***Sd***	***(n=3)***	***Sd***	**Saint Emilion limestone**	***Lavoux Limestone***
Ag	<LD	0.01	<0.00	0.01	<0.00	0.01	<0.00	0.04	0.02
As	17.08	3.97	1.72	3.15	1.68	4.79	1.61	9.42	1.26
Ba	1305.50	5.64	1.31	5.62	0.21	5.65	2.06	35.94	2.23
Be	<LD	<LD	<LD	<LD	<LD	<LD	<LD	ND	ND
Cd	0.35	0.24	0.08	0.24	0.13	0.24	0.03	0.89	0.41
Co	4.65	0.85	0.39	0.51	0.13	1.18	0.16	1.61	0.74
Cr	<LD	1.01	0.50	1.19	0.72	0.83	1.15	13.58	9.32
Cu	22.18	3.67	2.44	2.40	2.13	4.95	2.35	4.93	1.27
Fe	57.88	233.16	95.13	256.91	128.57	209.41	66.34	3981.65	1347.74
Ga	116.04	1.71	0.82	2.17	0.07	1.26	1.08	ND	ND
In	<LD	7.25	8.08	3.85	5.04	9.51	9.93	ND	ND
Li	2.12	0.61	0.15	0.60	0.16	0.61	0.18	ND	ND
Mn	23.46	58.53	14.08	51.28	18.20	65.78	2.62	282.80	33.41
Mo	5.01	0.06	0.03	0.04	0.01	0.08	0.02	ND	ND
Ni	<LD	2.32	0.65	1.86	0.53	2.78	0.37	6.68	5.80
Pb	6.18	1.98	0.50	1.83	0.57	2.13	0.47	5.09	0.43
Sb	2.53	0.14	0.05	0.11	0.05	0.17	0.04	0.24	0.05
Se	15.90	7.15	3.45	8.02	4.34	6.28	2.92	0.93	1.77
Si	2410.60	158.22	78.40	132.28	112.78	184.16	25.11	ND	ND
Sr	224.26	34.59	5.39	30.40	4.09	38.79	1.81	180.90	160.76
V	11.92	5.84	1.99	4.79	0.46	6.89	2.53	30.98	5.75
Zn	595.53	4.25	0.87	3.92	0.99	4.57	0.77	17.33	30.34

Table 4

Tab.4: Values on the left are the maximums concentrations of trace elements dissolved concentrations in the injection well F1. These values are compared with the quality standards for drinking water according to annex I of the decree of January 11th, 2007, relating to the limits and quality references of raw water and water intended for human consumption modified by the decree of August 4th, 2017, and the decree of December 9th, 2015 (INERIS, 2018) and guide values assigned to natural chemicals whose presence in drinking water is important from a health point of view (WHO, 2017). These values are also compared to the recommended maximum concentrations of trace elements in irrigation waters. These quality references are for water used continuously on all soils (Ayers and Westcot, 1976). The <LD symbol is used to denote values under detection limits. The symbol "-" indicates that no data has been found for this element.

(µg/L)	F1 Maximum ETM dissolved	INERIS, 2018	WHO, 2017	Ayers and Westcot, 1976
Ag	<LD	-	-	-
As	23.9	10	10	100
Ba	1305.5	700	700	-
Be	<LD	-	-	100
Cd	0.7	5	3	10
Co	6.4	-	-	50
Cr	<LD	50	50	100
Cu	36.9	2000	2000	200
Fe	88.0	200	-	5000
Ga	116.0	-	-	-
In	<LD	-	-	-
Li	2.1	-	-	2500
Mn	23.9	50	-	200
Mo	5.5	-	-	10
Ni	<LD	20	70	200
Pb	7.6	10	10	5000
Sb	2.5	5	20	-
Se	15.9	10	40	20
Si	2410.6	-	-	-
Sr	224.3	-	-	-
V	11.9	-	-	100
Zn	1582.9	-	-	2000